Chapter 4

Design of an experimental installation for the SunDial

The ASTEP system is constituted by the novel solar collector, the SunDial, and an innovative strategy to supply heat at different power and temperature levels. The level is set depending on the energy level available in the system, measured with the outlet temperature of the TES. In the previous chapter, the series configuration was selected for ASTEP due to the simplified control and the fewer elements required. The simulations carried out by the dynamic model have proven the effectiveness of the control system designed for the ASTEP system, including an innovative azimuthal defocus controller for the SunDial.

This chapter aims to prove that the ASTEP system performance matches the dynamic simulation's prediction and the expected performance before installation in the factory. Therefore, a testing facility is designed and built on a site owned by the Universidad Politecnica de Madrid, where the SunDial collectors are being constructed. The TES storage is being built in a different university and will be sent directly to the end-users, thus, the testing facility will count on an air-cooler to extract the heat produced by the SunDials. A control will be designed to simulate the heat extraction equal to the functioning of the TES in charge mode. Finally, the heat supply in levels to demand will be reproduced by a second air-cooler and a PI controller designed to accomplish the objective.

Therefore, the main goals of this chapter can be resumed in the next items:

- Design a testing facility to operate the SunDials with the control strategy planned for the end-users.
- Design two PI controllers to replicate the operation of the TES in model charge and the level demand with two different air-coolers.
- Design a set of experiments to evaluate the performance of the SunDials and the control strategy.
- Developed a methodology to validate the dynamic model.

4.1 Design of the test installation

The primary aim of the experimental setup situated in Tecnogetafe, Madrid is to operate the prototypes of SunDial-HL and SunDial-LL and validate the control strategy before sending these solar collectors to the end-users. To achieve this objective, an installation is designed to replicate the operation of SunDial as if it was providing heat to the factories. However, due to the ongoing development of the TES by a partner of the ASTEP project, simultaneous testing with the thermal storage is not feasible. As an alternative, an air cooler will be utilized to simulate TES operation in charge mode only. Additionally, a second air cooler will represent the process heat exchanger; both air coolers will feature a fan with speed control capability for managing extracted heat output as required.

Figure 4.1 shows the layout of the experimental test ring for the SunDials, where it is seen that both SunDials share the same balance of plant (BOP). Hence, the SunDials can not be tested simultaneously. The balance of plant counts with an inlet and outlet manifold with gate valves that permit the isolation of one of the SunDials.

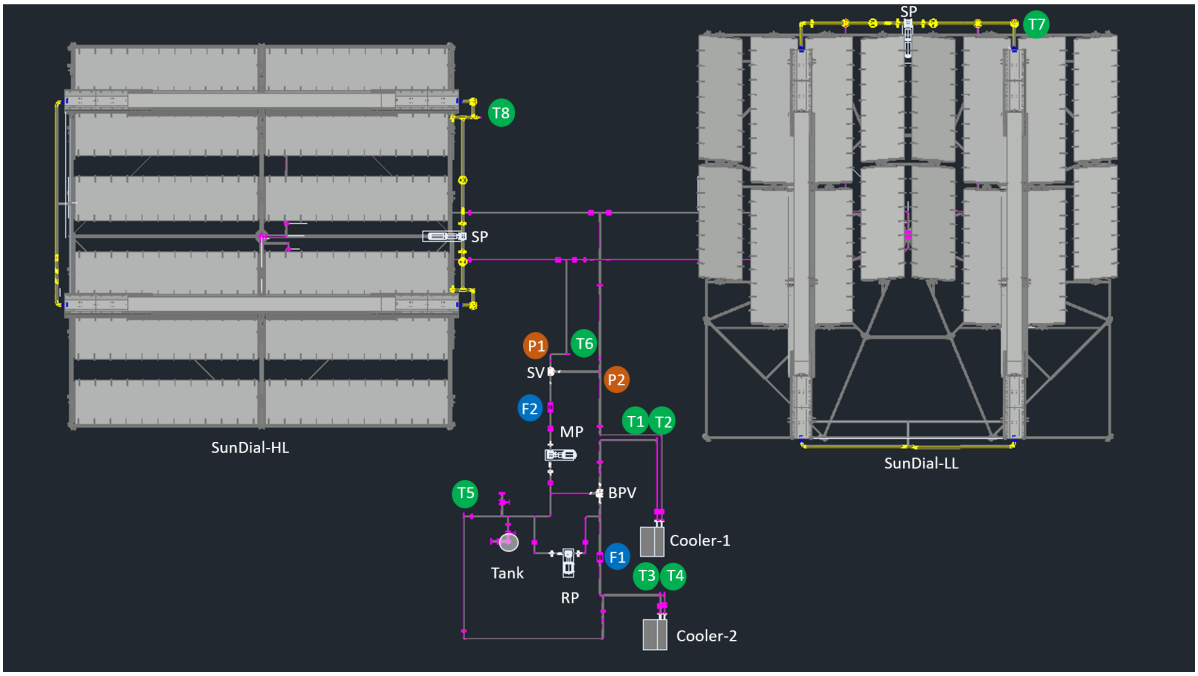

Figure 4.1: Layout of the experimental installation

Figure 4.2 illustrates the system flow diagram when one SunDial is connected. The power generated by the SunDial and the power extracted by the air coolers can be computed using temperature measurements at the inlet and outlet, along with the mass flow sensors, located at the inlet of the SunDial (F2) and the demand cooler (F1). The inlet temperature to the demand cooler (T3) is regulated by a PI controller using a recirculation pump (RP). At the same time, the mass flow is fixed with another PI and a bypass valve (BPV). The SunDial has a recirculation pump (SP) that fixes the flow through the receiver and a defocus controller to limit the maximum temperature to 240 °C. The power extracted by the air coolers is

controlled using a PI through airflow variation with a fan. The flow through the BOP to the SunDials is fixed by the main pump (MP). The installation also counts with an expansion tank that equalizes the pressure changes due to the thermal expansion of the thermal oil. A detailed presentation of all the installation components is in Section 4.1.1 and the control strategy is in Section 4.1.3. A more detailed diagram is presented in Appendix B where the piping & instrument diagrams for both SunDials and the BOP are presented. This diagram indicates all the equipment, instruments, actuators, and controllers.

All the measurement sensors, except for the meteorological station, are identified in the layout. Table 4.1 shows the list of the equipment and sensors represented in the layout. The meteorological station counts with an ambient temperature sensor, a wind sensor, and two Kipp & Zonen pyranometers. One of the pyranometers is used to sense the global component of the solar irradiation and the other has a shadow ring to measure the diffuse radiation. Then the direct normal irradiation can be calculated with these two values.

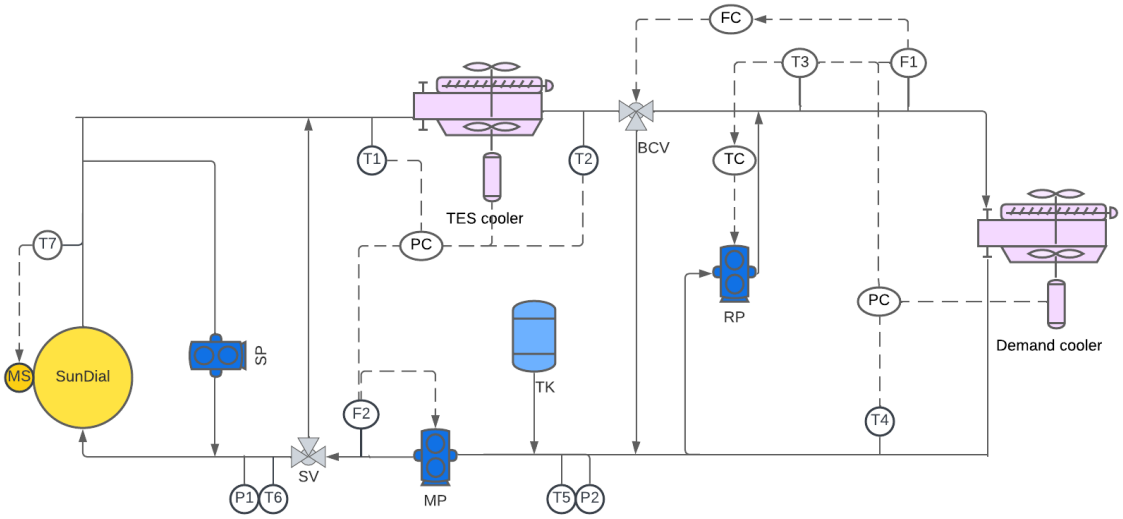

Figure 4.2: Flow diagram for the experimental installation

Figure 4.3 shows two pictures of the installation being built in Madrid. In the picture above, the front side of SunDials is shown, the SunDial-LL is on the left, and the SunDial-HL is on the right. The photo below shows the back side of the installation with the BOP in the middle of both solar collectors. Figure 4.4 shows a zoom-out of the BOP, where the two air coolers and the expansion tank are identified. From the picture, it can be seen that all the components of the balance of the plant are installed one meter above the ground. This is to prevent damage to the installation due to flooding. During the construction period, two floods occurred due to the overflow of a nearby river caused by historical rain in Madrid. After the severe damages produced to the installation by the floods on both occasions, it was decided to elevate the BOP.

Operating conditions

The idea is that the testing facility can operate in the same conditions for the end-users, this conditions were calculated with the dynamic model explained in Chapter 3. The BOP will be

(a)

(b)

Figure 4.3: Pictures of the experimental installation (a) front of the solar collectors, (b) back and balance of plant

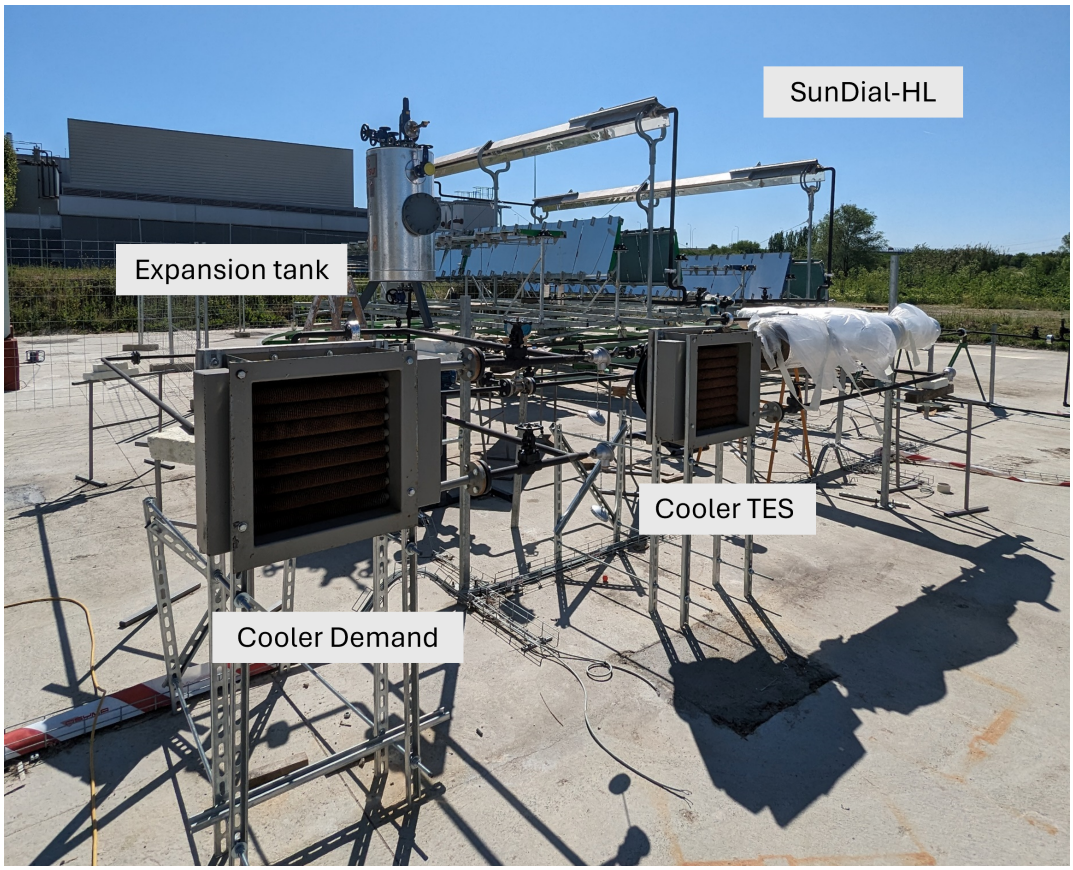

Figure 4.4: Picture of the BOP

Table 4.1: Instruments and equipment in the experimental installation.

Name	Abbreviation
SunDial pump	SP
Main pump	MP
Recirculation pump	RP
SunDial bypass valve	SV
Bypass control valve	BCV
Expansion tank	Tank
Cooler-1 inlet temperature sensor	T1
Cooler-1 outlet temperature sensor	T2
Cooler-2 inlet temperature sensor	T3
Cooler-2 outlet temperature sensor	T4
Tank temperature sensor	T5
BOP inlet temperature sensor	T6
SunDial-LL outlet temperature sensor	T7
SunDial-HL outlet temperature sensor	T8
BOP inlet pressure sensor	P1
BOP outlet pressure sensor	P2
Main pump flow sensor	F2
Demand flow sensor	F1

shared by the two SunDials, so it has to be allowed to operate in the conditions of the two end-users. The dairy factory results are depicted in Table 4.2 and the tube steel factory in Table 4.3. The maximum and minimum ranges for the conditions of the two industrial plants are illustrated in the tables. By comparing the ranges for the two factories it is noticed that most of the conditions are similar except for the temperature at the HX which is higher in the tube steel installation. However, the maximum operating temperature of 240 °C is equal for both end-users, and the maximum pressure of 3.65 bar is achieved in the outlet of the main pump. With this information, the piping can be mechanically designed, the methodology is shown in Appendix C.

4.1.1 Equipment & instruments

This section presents a full description of the equipment and instruments acquired to build the balance of plant. The principal components of the installation are the SunDials, but they are not included in this list, because they were previously introduced in Chapter 2. Hence, the focus will be put on the components of the balance of plant. All the components available in Spain were purchased locally to reduce the greenhouse emissions due to transportation and favor the local industry.

Coolers

The installation is equipped with two air coolers to simulate the operation of the TES in

Table 4.2: Operative conditions for the dairy factory and SunDial-LL

Component	Flow (kg/s)	Flow (m^3/h)	T (°C)	Pressure (bar)
Sundial	2.9-3.44	12.62-14.96	80-240	2.80-3.65
TES	0.54	2.35	190-240	1.50-2.95
HX	0.23	1.00	190-205	1.50-2.45
Tank			25-220	1.50-2.50
SP	2.9	12.62	80-240	1.65-3.65
MP	0.54	2.35	185-235	1.5-3.67
RP	0-0.19	0-0.83	170-195	1.5-2.60
SV	0.54	2.35	185-240	2.80-3.67
BPV	in:0.54	in:2.35	190-240	1.50-2.60
	out1: 0.04-0.23	out1: 0.17-1.00		
	out2: 0.24-0.54	out2: 1.04-2.35		

Table 4.3: Operative conditions for the tube steel factory and SunDial-HL

Component	Flow (kg/s)	Flow (m^3/h)	T (°C)	Pressure (bar)
Sundial	2.90-3.44	12.62-14.96	80-240	2.63-3.42
TES	0.54	2.35	190-240	1.65-2.62
HX	0.23	1.00	190-220	1.50-1.65
Tank			25-220	1.5-2.5
SP	2.9	12.62	80-240	1.50-3.42
MP	0.54	2.35	194-240	1.5-3.42
RP	0-0.10	0-0.43	192-207	1.5-1.64
SV	0.54	2.35	190-240	2.80-3.67
BPV	in:0.54	in:2.35	194-240	1.50-2.60
	out1: 0.13-0.23	out1: 0.57-1.00		
	out2: 0.24-0.54	out2: 1.04-2.35		

charge mode and the demand heat exchangers. The principal parameters of the air coolers are presented in Table 4.4. The demand air cooler was designed to extract the nominal power from both HXs plus an additional 10% under worst conditions, characterized by a lower HTF fluid temperature and higher ambient temperature. The TES air cooler's nominal power can extract SunDial's nominal power minus the power extracted from one demand HX. Both air coolers are fitted with a fan featuring a frequency driver that allows regulation of heat extraction capacity.

Table 4.4: Parameters of the air-coolers

Air-Cooler	TES	Demand
Power thermal (kW)	17.9	15.4
Air mass flow (kg/s)	0.48	0.48
Air temperature (°C)	35	35
HTF mass flow (kg/s)	0.52	0.23
HTF temperature (°C)	190	190
Fan Power (kW)	0.09	0.09

Pumps

The system is equipped with four gear pumps, including two identical SunDial recirculation pumps (SP) located above the platform. The main pump (MP) in the BOP circulates fluid from the BOP to the SunDial. Additionally, a recirculation pump (RP) is utilized to regulate the inlet temperature by recycling the cold fluid outlet of the demand cooler to reduce it. Table 4.5 illustrates the operational requirements for these pumps. Each gear pump features an integrated bypass to prevent over-pressure, a Y filter to safeguard against pump damage, and gate valves at both inlet and outlet points for maintenance isolation purposes. These gear pumps are fitted with packing seals capable of resisting temperatures up to 250 °C and their flow can be controlled using frequency drivers. While MP and SP operate at a fixed flow rate, RP's operation varies based on PI controller instructions.

Table 4.5: Parameters of the pumps

Pump	MP	SP	RP
Nominal mass flow (kg/s)	0.54	3.46	0-0.19
Nominal Flow (l/min)	38.28-39.6	204-216	0-13.83
Temperature (°C)	190-230	180-240	180-206
Inlet pressure (bar)	1.5	2.28-2.85	1.5
Outlet pressure (bar)	3.7-4.3	2.9-3.6	2.5-3.1
Nominal pressure drop (bar)	2.2-2.8	0.7-0.8	1-1.6
Power (kW)	1.5	5.5	0.75
Flow at 1450 rpm (l/min)	48	265	20
P max. (bar)	7	4	7

Expansion Tank

An expansion tank is necessary to equalize the pressure in the system due to variations in thermal oil volume with temperature. The expansion tank is located at the highest point of the BOP, but since the SunDial receivers are situated even higher, this means that the vent point of the installation should be on the SunDials. The thermal oil undergoes oxidation when it is exposed to air, this oxidation causes solid formation and fouling reducing the heat transference effectiveness. Hence, an effective method to reduce oxidation is to blanket the expansion tank with an inert gas (Nitrogen). The pressure of the tank has to be over the atmospheric to prevent air entrance to the tank, thus, it is set between 1.5 and 2.5 barg. An auto-regulated valve controls inlet flow from a nitrogen tank, followed by a spring-loaded pressure relief valve set at 2.5 barg to release excess pressure as needed. Additionally, there are two level switches to indicate when minimum and maximum levels have been reached, each playing specific safety roles detailed in section 4.1.5, where the safety actions related to the control system are explained.

The volume of the expansion tank is determined by calculating the difference in fluid volume between operational and shut-down conditions. The fluid inventory, outlined in Table 4.6, includes the SunDials' volume, system piping, and coolers, with a total installation volume of 217 liters. Cold and hot mass is obtained by multiplying the total mass with the corresponding density. The difference between these masses multiplied by the ambient temperature's density yields the minimum expansion tank volume of 32.4 liters. To accommodate working within 25-75 % of the total level, twice this minimum capacity (65 l) was needed for acquiring an expansion tank size of 70 liters.

Table 4.6: Parameter to calculate the expansion tank volume

Parameter	Value
Piping (l)	102
Sundials (l)	110
Coolers (l)	6
Density 240 °C	807
Density 10 °C	978
Hot mass 240 °C (kg)	149
Cold mass 10 °C (kg)	181

Control valves

The BOP has a control valve that is designed to regulate the mass flow as needed by diverting excess flow from the air cooler. This action is necessary because the main pump sets the flow at 0.54 kg/s, while the demand requires for a lower mass flow of 0.23 kg/s. Additionally, there is an ON/OFF valve to bypass the SunDials and recirculate only through the BOP. The control valves are equipped with an electrical actuator which will be controlled by the system. The operating parameters of these valves can be seen in Table 4.7.

Rotatory Joints

The connection between the static piping from the balance of plant and the moving SunDial platform is a particularly complex aspect of the system. Rotary joints, located at the center

Table 4.7: Parameters for the bypass control valve

Parameter	BPV			SV
	inlet	outlet 1	outlet 2	
Nominal mass flow (kg/s)	0.54	0.31-0.54	0-0.23	0.54
Nominal Flow (m^3/h)	2.35	1.34-2.35	0-1.00	2.35
Nominal Flow (l/min)	39.1	22.33-39.1	0-16.7	39.1
Temperature (°C)	190-240	190-240	190-240	194-240
Pressure (bar)	3.12	2.92	3.02	3.77
Nominal pressure drop (bar)		0.2	0.1	3.67

of rotation of the SunDial, facilitate this connection. The piping rises from below the SunDial platform through a central column that supports it, as depicted in Figure 4.5. The rotary joints are aligned one above another on this same line. To prevent tension and potential malfunctioning or leakages in these rotary joints, one of the connections is made using a flexible hose. This specific rotary joint is constructed with graphite impregnated with an antimony seal designed to withstand high temperatures while working with thermal oil.

Pressure Safety Valve

The SunDials require a pressure safety valve to prevent overpressure. This could occur if the manual valves in the inlet and outlet manifolds of the balance of plant are operated incorrectly, isolating the SunDial from the expansion vessel. These valves connect or disconnect each SunDial to/from the BOP for testing. If accidentally isolated from the expansion vessel, heating of fluid may occur if the collector is in a focus position, leading to overpressure due to confined liquid thermal expansion. Valves typically used for this scenario have a size of 3/4" x 1".

The relief pressure of the PSV has to be equal to the design pressure of the weakest element in the SunDial. Table 4.8 shows the values for the design pressure of the elements of the SunDial, where the pipings are the weakest element. The piping mechanical design is shown in Appendix C, where the maximum pressure has been calculated using the standard UNE-EN 13480-3. Therefore, the relief pressure was set to 8 barg. Table 4.9 shows the data for the selected valve. However, the maximum operating pressure is 4 barg, thus, the facility has a secure coefficient of 2.

Table 4.8: Design pressure of SunDial elements

	Design Pressure [barg]
Receiver	46
SunDial Pump	25
Piping	8.29
Temperature sensors	16
Rotatory Joint	35
Vent valve automatic	125

Figure 4.5: Picture of the rotatory joint assembly

Table 4.9: Pressure relief valve characteristics

Parameter	Value
Orifice Designation	D - 0.110 in^2
Inlet size	1/2 in
Outlet size	1 in
Set pressure	8 barg
Max. relief capacity	8.7 m^3/h

Sensors

The installation counts with sensors that are used to monitor the operation conditions, provide information to the control system, and record data to calculate performance indicators that will be introduced in section 4.2.1. The main variables to measure are temperature, flow, and DNI, the uncertainty of the instruments is illustrated in Table 4.10. All the sensors present in the installation are represented in layout Figure 4.1 and are tagged with the nomenclature of Table 4.1.

Platinum thermoresistance temperature sensors were chosen for their high accuracy and minimal interference. The PT100 is calibrated for temperatures ranging from -20 °C to 260 °C, with a precision of 0.3 at 0 °C and 0.8 at 100 °C. There are a total of eight temperature sensors, with the most critical ones being T8 and T7 located at the outlet of the SunDials. The inlet temperature sensor (T6), situated in the BOP, is shared by the SunDials. These sensor readings are essential for calculating SunDial power and controlling maximum outlet temperature. The demand cooler intel temperature (T3) is controlled to a specific set point, and the outlet temperature of the TES (T2) is used to select in which mode the system has to operate. Finally, the inlet and outlet temperature of the air coolers are used to calculate the extracted power.

Flow measurement is conducted using a vortex flow meter, known for its volumetric precision of less than 1 %. One flowmeter is needed to sense the demand flow control by the bypass valve. The second flowmeter is utilized to measure the flow from the main pump directed to the SunDial and the TES air cooler.

Two pressure transmitters are used to measure the loss of pressure of the installation with a range between 0 and 6 bar. Finally, the expansion tank counts with a manometer with local pressure indication and two level switches to send a signal to the control system in case the high or low level has been reached.

The ambient conditions are also important for the model validation and the control of the system so a meteorological station with data on ambient temperature, and wind velocity was installed. The wind velocity is required for the control system to move the SunDial to a safe position in case of high velocity. This will be further explained in section 4.1.5.

The direct normal irradiation is essential for calculating the performance of the SunDial and validating the ASTEP model presented in Chapter 3. While a pyrheliometer can be used to measure DNI, it is expensive and requires intensive maintenance. An alternative approach involves using two pyranometers: one for measuring global DNI and another for measuring diffuse radiation with the help of a shadow ring, which blocks the direct component. By utilizing Equation 4.1, DNI can then be calculated. The SMP10 Kipp&Zonen pyranometer, used for this purpose, has an uncertainty of 3 %.

$$G = \mathrm{DNI} \cdot cos(\theta_z) + D \tag{4.1}$$

Table 4.10: Instruments uncertainty

Sensors	Uncertainty (%)
Temperature	0.5
Flow	1
Pyranometers	3

4.1.2 SCADA

The installation counts with a Supervisory Control and Data Acquisition system (SCADA), which will be in charge of controlling the operation of the system automatically and recording all the variables that are measured in the experimental installation. Table 4.11 presents the list of variables acquired with a time interval of 1 minute.

Table 4.11: List of the data records in the acquisition system

Acronym	Description
T1 to T8	Temperature sensor
P1 to P2	Pressure sensor
F1 to F2	Flow meter
FAN1 to FAN2	Fan frequency driver
SP-LL	Pump frequency driver
SP-HL	Pump frequency driver
MP	Pump frequency driver
RP	Pump frequency driver
M1-LL 2 units	Platform motor frequency driver
M2-HL 2 units	Platform motor frequency driver
M3 a M9	Mirrors motors frequency driver
SV	On/off valve
BPV	Control Valve
Vv-LL	On/off vent valve
Vv-HL	On/off vent valve
Fill-Pump	Pump frequency
LSL-10	Low level switch
HSL-10	High level switch
G	Global irradiation
D	Diffuse irradiation
T_{amb}	Ambient temperature
v_{wind}	Wind velocity
d_{wind}	Wind direction

4.1.3 Control strategy for the experimental installation

The control strategy of the experimental installation aims to replicate the operation of the end-users (Section 2.2.1). However, this control strategy needs to be updated due to the absence of the TES, which has been substituted with an air cooler, and the replacement of the demand HX with a second air cooler.

The control flow diagram for the experimental installation is illustrated in Figure 4.7. The power extracted by the demand cooler will be controlled by a PI controller and the frequency driver, which regulates the velocity of the fan. This air cooler could function at different setpoints to mimic the operation of one HX or both. Consequently, how the demand air cooler operates will vary depending on whether it simulates the dairy factory and SunDial-LL or the tube steel factory and SunDial-HL. For instance, for the dairy factory, 6 kW, 8 kW, or 14 kW of power will be required while for the tube steel factory, it would be 7 kW and 14 kW.

The first difference with the end-user installation is that the power extracted by the demand cooler will depend on the outlet temperature of the TES cooler and the prior state of the demand cooler. The prior state of the demand air cooler is determined by the temperature difference between the inlet and the outlet, using temperature sensors T3 and T4. This temperature difference directly influences the power extraction from the demand cooler by Eq. 4.2. The HTF mass flow rate circulating through the demand cooler remains constant and is regulated by a PI controller with the bypass valve (BPV).

$$P_{\text{cooler}} = \dot{m}_{\text{cooler}} \cdot c_p \cdot (T_{\text{out,cooler}} - T_{\text{in,cooler}}) \tag{4.2}$$

Tables 4.12 and 4.14 depicted the setpoints for the temperature difference for the demand cooler in the dairy factory operation, the former is for when the factory is open between 9 AM to 5 PM, and the latter is for when it is closed. The difference between these tables is that when the factory is closed only the chiller is active. The setpoint will depend on the temperature difference in the demand cooler in the previous time recorded by the control system ($dT_{\text{demand,cooler}}{}^{\text{t-1}}$) and the outlet temperature of the TES cooler. It is observed from Table 4.12 that a higher outlet temperature of the TES cooler results in a higher delta of temperature being selected for the demand cooler. In the case of the tube steel factory, only one Table 4.15 is required due to the operation being independent of the hours of the day.

A PI will also control the power extracted by the TES cooler. This PI will control the TES cooler outlet temperature to follow a thermal profile dependent on the inlet temperature of the TES cooler. Figure 4.6a illustrates the inlet and outlet temperature of the TES versus the sample time for a Summer day. The outlet temperature of the TES can be characterized in three sections, which can be represented as linear functions. Furthermore, when the outlet temperature reaches the phase change temperature 222 ° C the temperature remains constant. Thus, the speed of the fan will be managed to control the outlet temperature of the TES cooler to a setpoint that can be calculated with the Equations 4.3. These equations are dependent on the inlet temperature of the TES cooler.

Table 4.12: Temperature setpoints for the demand cooler when the dairy factory is open

$dT_{demand,cooler}^{t-1}$	TES-cooler outlet temperature				
	<205°C	205°C-210°C	210°C-220°C	220°C-225°C	>225°C
0	None	None	15	15	26
15	None	15	15	15	26
11	None	None	15	15	26
26	None	15	15	26	26

Table 4.14: Temperature setpoints for the demand cooler when the dairy factory is closed.

$dT_{demand,cooler}^{t-1}$	TES-cooler outlet temperature		
	<190°C	190°C-200°C	>200°C
0	None	None	11
11	None	11	11

Table 4.15: Temperature setpoints for the demand cooler for the tube steel factory.

$dT_{demand,cooler}^{t-1}$	TES-cooler outlet temperature				
	<205°C	205°C-210°C	210°C-220°C	220°C-225°C	>225°C
0	0	0	13	13	26
13	0	13	13	13	26
26	0	13	13	26	26

$$
\begin{aligned}
T_{\text{in}} - T_{\text{out}} &= -0.594 \cdot T_{\text{in}} + 112, T_{\text{in,TES}} < 205°C \\
T_{\text{in}} - T_{\text{out}} &= -0.292 \cdot T_{\text{in}} + 53, T_{\text{in,TES}} < 230°C \\
T_{\text{in}} - T_{\text{out}} &= -10, T_{\text{in,TES}} >= 230°C
\end{aligned} \tag{4.3}
$$

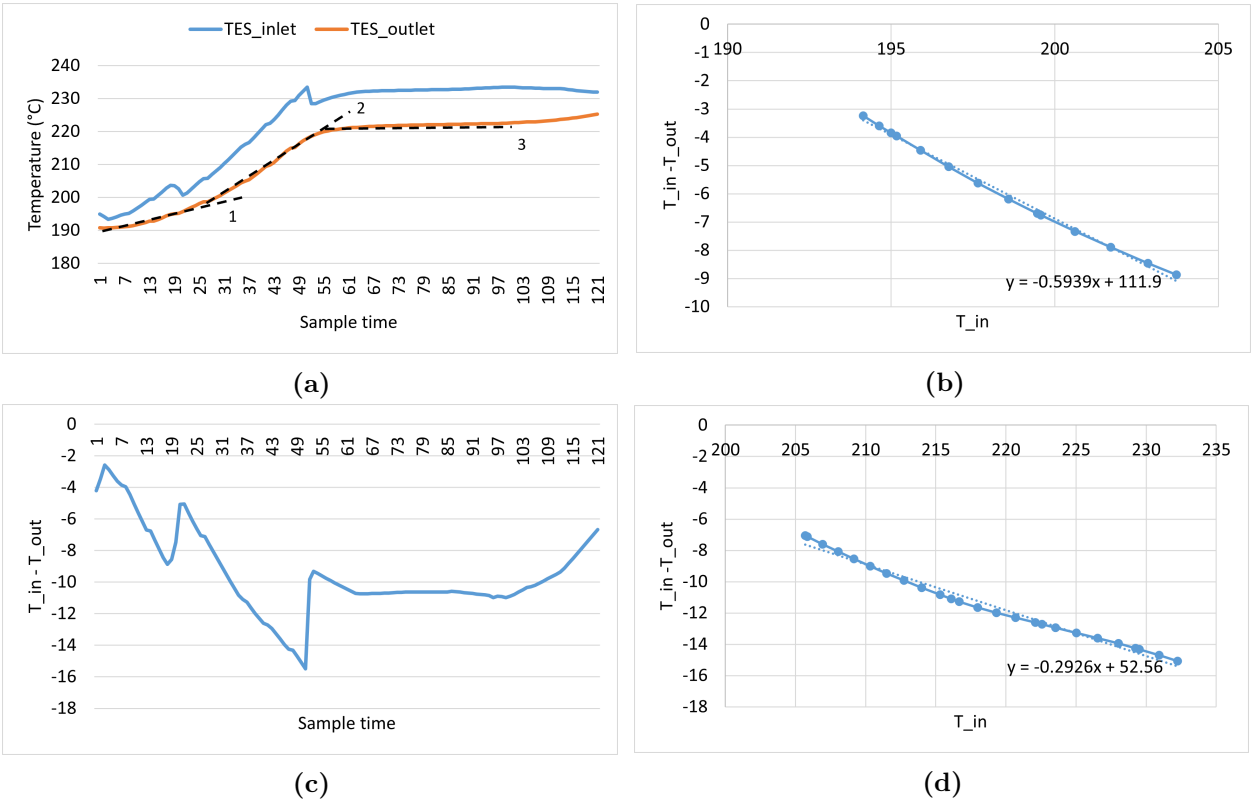

(a) **(b)** **(c)** **(d)**

Figure 4.6: (a) TES inlet and outlet temperature versus sample time, (d) TES inlet temperature minus TES outlet temperature versus TES inlet temperature until 205 °C, (c) TES inlet temperature minus TES outlet temperature versus sample time, (d) TES inlet temperature minus TES outlet temperature versus TES inlet temperature until 230 °C.

The start-up procedure is depicted in Figure 4.8. The SunDial pre-heating is completed when the outlet temperature achieves the process's start-up setpoint specified in Table 4.17. The pre-heating is carried out by recirculating flow through the balance or plant with the air cooler fans turned off to increase the temperature of the whole system gradually and avoid thermal stresses. Then, the demand cooler will start up when the outlet temperature of the TES cooler meets the process setpoint. Finally, TES cooler will begin operation when the power generated by SunDial exceeds the power extracted by the demand cooler plus the thermal losses.

The shutdown sequence depicted in Figure 4.9 is similar to the implementation in the end-user installation, but with the difference that in the second stage of the shutdown, the air cooler fans are turned off.

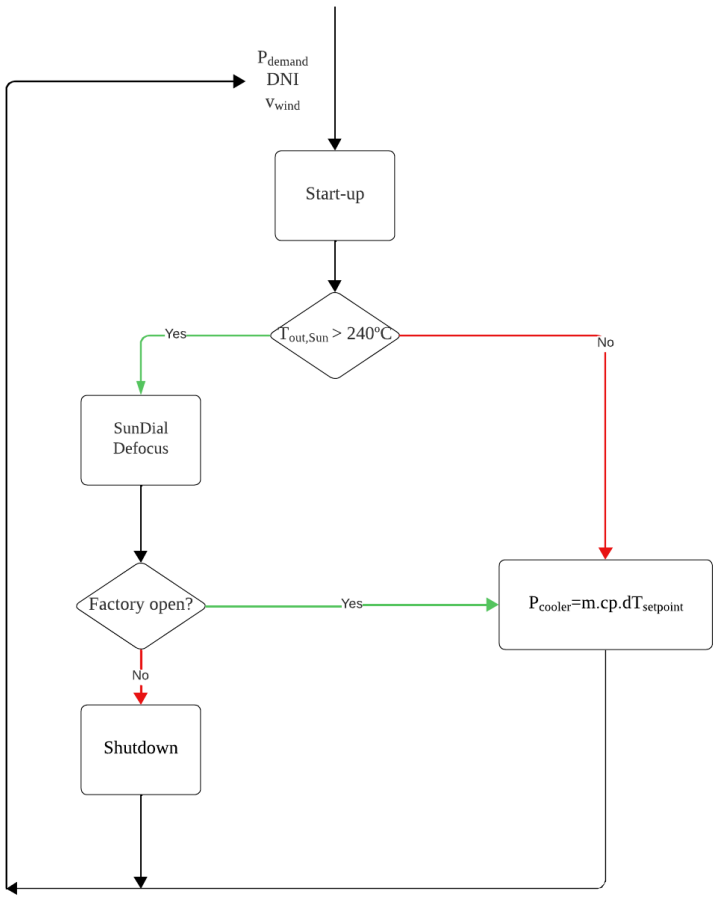

Figure 4.7: Start-up flow control strategy for experimental installation

Table 4.17: Start-up temperature setpoints for the processes

Process	Temperature setpoint
Dairy	if open 210°C if closed 195°C
Tube steel	210°C

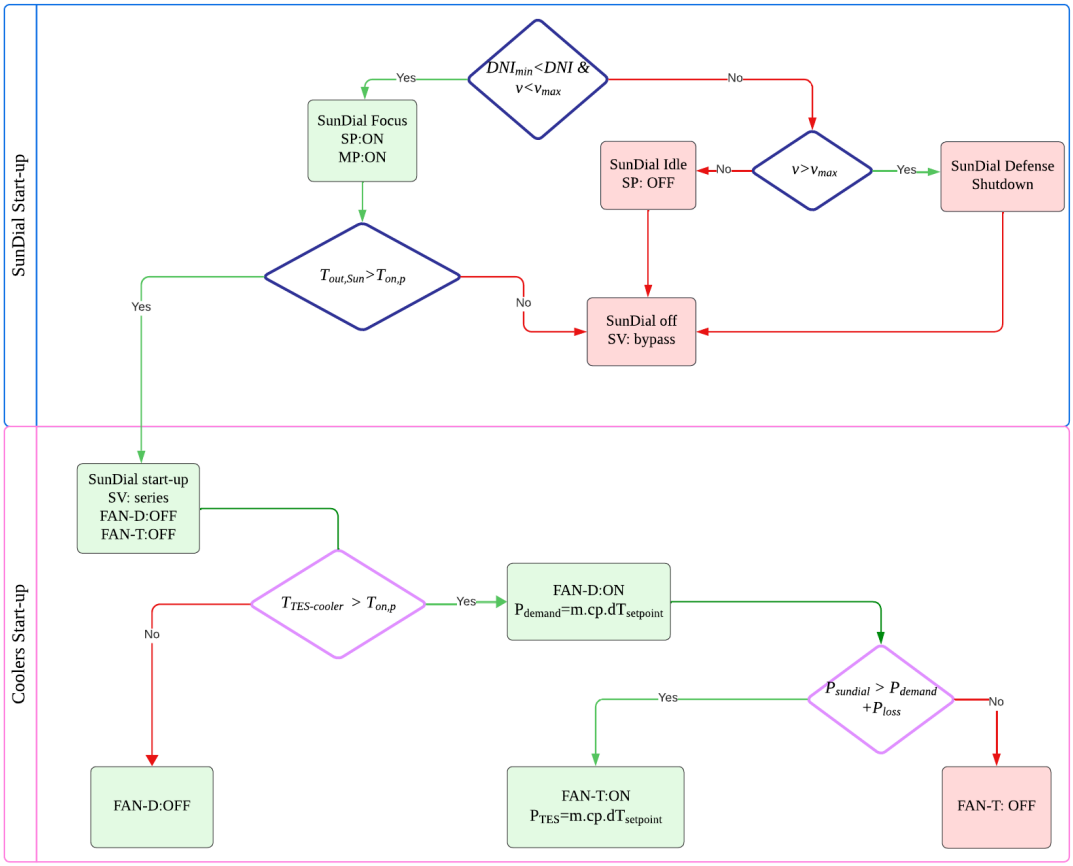

Figure 4.8: Start-up flow control strategy for experimental installation

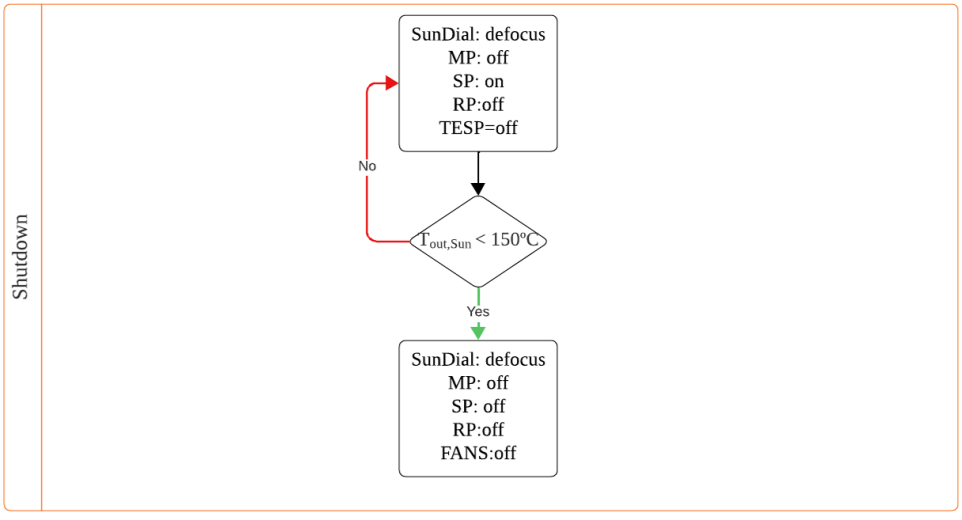

Figure 4.9: Shutdown flow control strategy for experimental installation

4.1.4 Designed of the air-coolers PI controllers

The PI controllers for the air-coolers were designed by using the dynamic models developed in Section 3.1. However, the experimental installation in Madrid which is described in section 4.1 differs from the dynamic model designed in Chapter 3.1 principally due to the absence of thermal energy storage (TES). The Madrid installation counts with two air coolers to replicate the operation of the TES- only in charge mode- and the process heat exchangers. Figure 4.10 shows the Dymola model where the TES modules and the two heat exchangers of the demands have been replaced for two air coolers. Also, the whole pipes of the system were consolidated into two pipes: the SunDial pipe with a nominal diameter of 50 mm and a total longitude of 20 meters and the balance of plant with a nominal diameter of 20 mm and a total longitude of 40 meters.

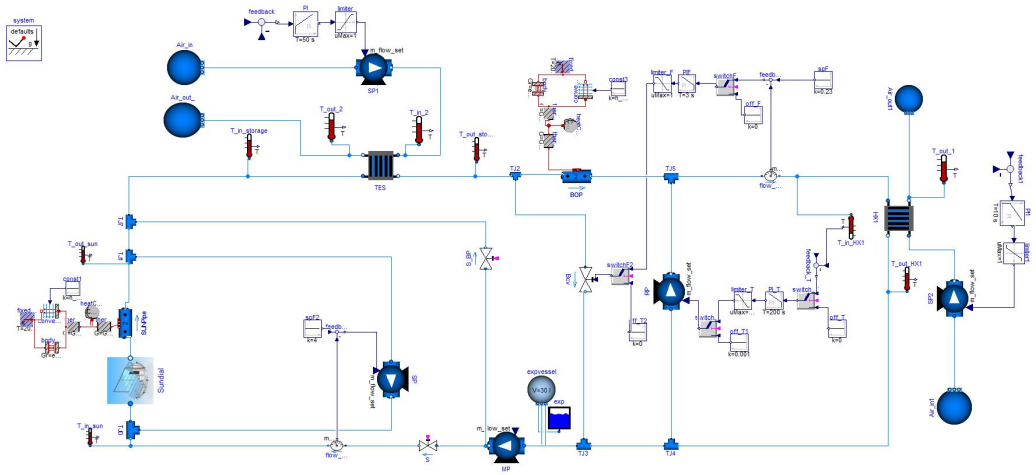

Figure 4.10: Screenshot of the Dymola model for the Getafe installation

The air coolers were modeled with the Buildings library model called Plate Heat Exchanger Effectiveness NTU [56]. This model calculates the heat transfer with the NTU method which calculates the heat transfer by the Eq. 4.4 and the heat transfer effectiveness (Eq. 4.5) depends on the number of transfer units (NTU), the flow regime- in this case, cross flow- and the ratio of minimum to maximum capacity (Z). The air is modeled with Modelica Simple Air, which is an ideal gas model for low temperatures. The parameters introduced to the air cooler model are shown in Table 4.18.

$$Q = Q_{\max}\epsilon \tag{4.4}$$

$$\epsilon = f(\text{NTU}, Z, \text{flow regime}) \tag{4.5}$$

The air cooler's control is achieved by varying the airflow with a frequency driver that regulates the fan's speed. The fan was modeled using a Modelica control pump and is controlled by a proportional integrative controller, which regulates the flow of air through the HX. The control strategy implemented is the one described in the previous section (4.1.3) in which

Table 4.18: Parameters of the Air cooler model

Parameter	Air cooler- TES	Air cooler - HX
m_{oil}[kg/s]	0.52	0.23
m_{air}[kg/s]	0.48	0.48
dP_{oil}[kPa]	18.6	12.7
dP_{air}[Pa]	39	39
$Q_{nominal}$[kW]	17.9	15.4
$T_{in,oil}$[°C]	190	190
$T_{in,air}$[°C]	35	35

the controller compares the power extracted by the air-cooler and the setpoint. The setpoints are calculated by multiplying the differential temperatures that were defined in the previous section in Tables 4.12 to 4.14 with the mass flow rate and specific heat. The controller variables were calculated with the Ziegler-Nichols and are shown in Table 4.19.

Table 4.19: Controller constants for the air coolers PI

Controller	K_c	T_c [s]	u_{max} [kg/s]	u_{min} [kg/s]
TES-cooler	0.04	50	1	0.01
Demad-cooler	0.04	10	1	0.01

4.1.5 Safety actions of the control system

The control system initiates automatic safety actions if the operative variable exceeds its normal value. These actions are activated by signals enumerated in Table 4.20. The shutdown routine involves stopping the main pump (MP), defocusing SunDial, and keeping the SunDial recirculation pump (SP) on until the outlet temperature of the SunDial decreases by 150 ºC. Additionally, an emergency shutdown button is available to stop the system in case of emergencies like fire or an HFT leakage.

Table 4.20: Safety actions of the control system

Signal	Action
High level in the expansion tank	Shutdown routine
Low level in the expansion tank	Shutdown routine
High pressure	Shutdown routine
High wind velocity	Move SunDial to the safe position (depends on the wind direction)
High temperature	Defocus SunDial

4.2 Definition of the experimental procedures

This section outlines the experiment design and the required tests for setting up the installation. Initially, the key performance indicators for assessing SunDial's performance and ASTEP system's control strategy functionality are introduced with an uncertainty and error propagation analysis. Secondly, a set of tests necessary to verify the installation is properly constructed and to prevent component damages during system commissioning is presented. Lastly, a description of the experiments to assess SunDial's performance and ASTEP control strategy is provided.

4.2.1 Key performance indicators, uncertainty, and error propagation

The performance of the SunDials is evaluated using three indicators: the outlet temperature, power generated, and efficiency. The power is calculated using Equations 4.6 and 4.7 based on data recorded by sensors. The efficiency of the SunDial is determined using Equation 4.8, with DNI calculated from measurements taken by pyranometers. The outlet temperature of the SunDial will be monitored using either sensors T8 or T7, depending on which specific SunDial is being tested. Additionally, the assessment of defocus controller performance will involve recording movement through an encoder and ensuring that outlet temperatures are maintained below maximum admissible levels. The correct functioning of this control is verified by identifying the time the outlet temperature is over the maximum setpoint.

$$P_{\text{sundial-hl}} = \dot{m}_{F2} \cdot c_p \cdot (T_8 - T_6) \tag{4.6}$$

$$P_{\text{sundial-ll}} = \dot{m}_{F2} \cdot c_p \cdot (T_7 - T_6) \tag{4.7}$$

$$\eta = \frac{P_{\text{sundial}}}{DNI \cdot A_r} \tag{4.8}$$

$$P_{\text{demand}} = \dot{m}_{F1} \cdot c_p \cdot (T_4 - T_3) \tag{4.9}$$

$$P_{\text{TES}} = \dot{m}_{F2} \cdot c_p \cdot (T_2 - T_1) \tag{4.10}$$

The control strategy is evaluated based on its ability to maintain the demand inlet temperature and mass flow at their setpoints, as well as its effectiveness in switching between different demand levels. The evaluation involves calculating the Mean Absolute Error between the temperature measured by T3 (at the inlet of the demand) and the setpoint when the installation is in demand feeding modes. Additionally, the power extracted by the demand air cooler is determined using measurements from sensors F1, T3, and T4 with Equation 4.9. The mass flow is maintained at a constant value and can be verified by sensor F1 (at the inlet of the demand). Lastly, verification of power extraction by the demand is confirmed through TES cooler outlet temperature measurement with sensor T2 (at the outlet of the TES).

The TES cooler's extracted power is determined using measurements from sensors F2, T1, and T2 with Equation 4.10 . As a result, the thermal losses are approximated through the

energy balance in Equation 4.11 once a steady state has been reached. Table 4.21 summarizes all key performance indicators, the corresponding sensors used for their calculation, and the calculated uncertainty for each KPI.

$$P_{\text{sundial}} = P_{\text{demand}} + P_{\text{TES}} + P_{\text{loss}} \tag{4.11}$$

Table 4.21: List of KPI and the associated sensors with the calculated uncertainty

KPI	sensors	Uncertainty
SunDial Power	T6-T8, and F2	1.1%
SunDial outlet temperatute	T7 orT8	0.5%
Sundial efficiency	G, D, T6-T8 and F2	3.2%
Demand inlet temperature	T3	0.5%
Power extracted by demand cooler	T3,T4, and F1	1.1%
Power extracted by TES cooler	T1,T2, and F2	1.1%
Thermal losses	Balance of energy	1.1%

The uncertainties of the sensor used to measure the variables required to calculate the KPIs were shown in Table 4.10. The uncertainty of each KPI can be calculated with the error propagation formula. For example, the uncertainty of the power is calculated with Equation 4.12, where sigma is the uncertainty of the variable. The uncertainty of the specific capacity is calculated with Equation 4.13 where b is the constant multiplying the temperature in the specific heat capacity equation shown in Appendix A. The uncertainty of the ΔT is equal to the temperature uncertainty. For the operative values of the SunDial, the power uncertainty result is approximately 1.1 %.

$$\left(\frac{\sigma_{\text{P}}}{P}\right)^2 = \left(\frac{\sigma_{\dot{m}}}{\dot{m}}\right)^2 + \left(\frac{\sigma_{\text{c}}}{c}\right)^2 + \left(\frac{\sigma_{\Delta\text{T}}}{\Delta T}\right)^2 \tag{4.12}$$

$$\sigma_{\text{c}} = b \cdot \sigma_{\text{T}} \tag{4.13}$$

The expected values of KPI were estimated with the dynamic model of Chapter 3 and are shown in Table 4.22. The KPIS can be divided into two categories, the ones related to the SunDial performance which are the three first, and the ones related to the control system, which are the next three. Finally, the thermal losses affected the two categories.

Regarding the SunDial KPIs, the expected values are theoretical estimations. Thus, the objective is to adjust these values to have a correct characterization of the SunDial. A complete failure of the test will involve not being able to strat-up the SunDial, or having a rupture of the receiver tube due to thermal stress. If the thermal losses of the system are significantly higher than the estimated this could prevent achieving the expected results of power supply to the demand compared to the simulations results.

Regarding the control system KPIs, the demand inlet temperature value depends on the factory being simulated and the outlet temperature of the TES cooler. A failure of this test will involve not managing to control the inlet temperature to the setpoints or not being able to switch between demand levels. The power extracted by the demand cooler also will be dependent on the TES cooler outlet temperature and the failure of the test will imply the system's incorrect switching between the different power levels or not being able to extract the correct amount. The power of the TES cooler is dependent on the inlet temperature and the set temperature profile by the linear equations, a failure of the experiment will involve the incapacity to extract the required heat and an overheating of the system, or higher extracting preventing the system temperature increase.

Table 4.22: Expected values for the KPIs calculated with the dynamic model

KPI	Expect value
SunDial Power	SunDial-LL peak 25 kW and SunDial-HL peak 20 kW
SunDial outlet temperatute	range between 190 °C and 240 °C
Sundial efficiency	between 0.45 and 0.52
Demand inlet temperature	190-205 and 220 °C
Power extracted by demand cooler	6, 7, 8 and 14 kW
Power extracted by TES cooler	between 1.7 kW and 17 kW
Thermal losses	15-30%

4.2.2 Commissioning

The commissioning phase includes all the necessary tests before start-up. The primary goal is to ensure that everything has been installed correctly to prevent malfunctions, errors in testing, and damage to components. The main tests conducted during this phase include:

- Leak test.
- Platform rotation test.
- Cold commissioning: system filling with HTF.
- Hot commissioning: pre-heating and controller tuning.

Leak test

This test is designed to ensure that all connections are properly sealed and that the system has no points of leakage. The system will be pressurized with air and checked for leaks. The elements in the system have different design pressures, as outlined in Table 4.23. Therefore, the leak test pressure must not exceed the design pressure of the element being tested. Leaks can be detected by monitoring the pressure over a period of time; if there is no decrease in pressure, it indicates that there are no leaks. However, if there is a pressure drop, potential leak locations can be identified by applying liquid soap to flanges and threads and looking for air bubbles. While this method successfully identifies thread leaks, it does not always detect

flange leaks. As a result, a second leak test involves filling the installation with oil to easily identify and fix any leaks present.

Table 4.23: Design pressure of the elements in the experimental installation

Element	Design pressure [barg]
Receiver	46
Pumps	25
Piping	8.29
Temperature sensors	16
Rotatory Joint	35
Vent valve	125
Pressure safety valve	8
Flow meters	40
Pressure sensors	40
Three-way valves	15
Coolers	12
Expansion tank	6

The installation can be subdivided into subsystems by valves and blind flanges to test separately at different pressures. Hence the system has been divided into the next subsystems to be tested:

- The rotatory joints are a critical area of the installation due to their challenging access in the middle of the platform and the presence of threaded connections. These components are tested individually by pressurizing them with 8 barg of air.
- The rest of the installation, except the expansion vessel, is pressurized first with air at 2 barg and then with oil at 4 barg.
- The expansion tank has a pressure relief valve set at 2.5 barg that can not be isolated, so the test pressure will be carried out to 2 barg.

Platform rotation test

This test is meant to prove the correct performance of the rotation of the platforms and the rotatory joints. A visual inspection is carried out to ensure that the wheels are properly mounted over the rotating path and that the rotatory joints have no stresses produced by the piping connections. The larger platform rotation azimuth angle required is 120° to follow the sun's position in the morning and afternoon. The limitation of the maximum rotation is imposed by the rotating joints' support that collides with the piping after the maximum azimuth is reached, as seen in Figure 4.11. The SunDial counts with sensors, equipment, and an internal PLC that must be connected to the electricity. Therefore, the cables from the elements above the platform need to be routed to the platform center to connect with the main power supply outside the platform. Thus, the cables need to come through a cable chain in the center of the platform that controls their movement when the platform is rotating to prevent damage. The platform rotating test includes the verification that all the cables are properly mounted through the center of the platform.

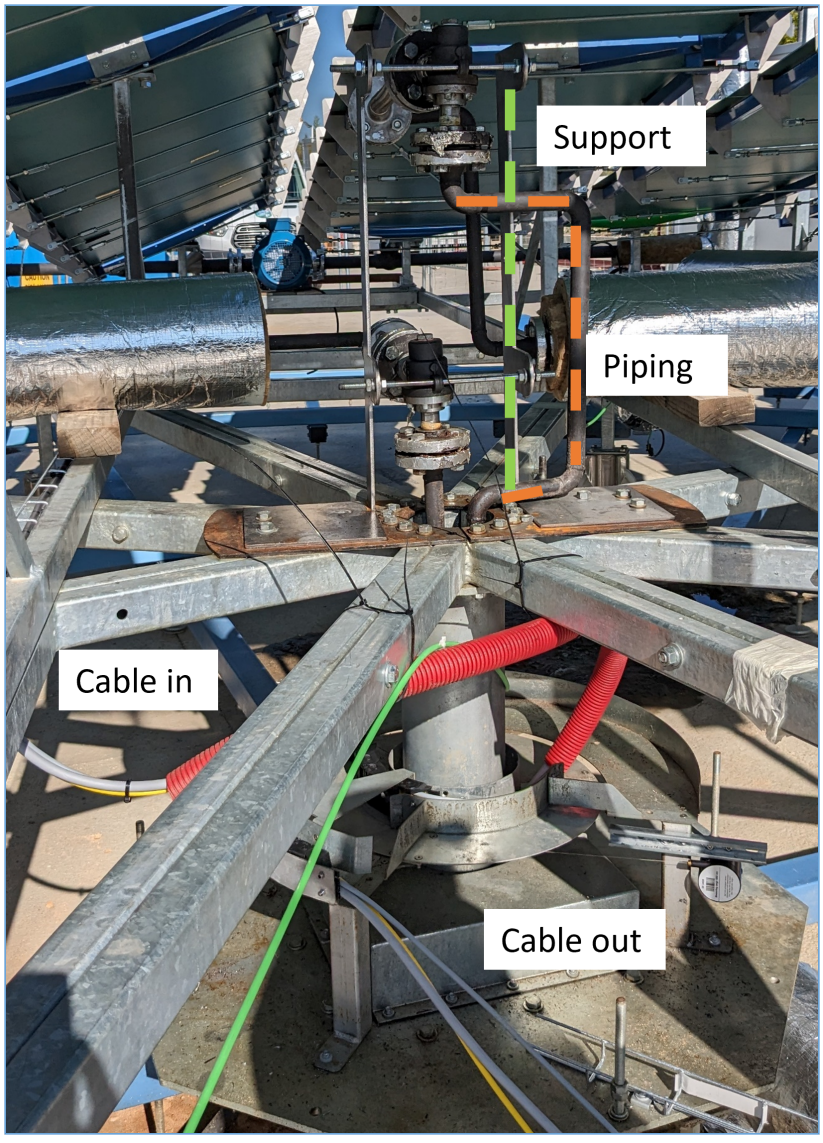

Figure 4.11: Photo of the center of the platform showing the rotating joints ensemble and the cables leaving the platform

Cold commissioning: system filling with heat transfer fluid

This test involves filling the system with heat transfer fluid, Therminol 59, and pressurizing the expansion tank with nitrogen. It is important to eliminate all air from the installation to prevent malfunctioning. Trapped air reduces heat transfer coefficients and can lead to cavitation in pumps and valves. Therefore, the initial step of cold commissioning will be air elimination.

The fill and drain manifold is illustrated in Figure 4.12 with the expansion tank and the manual valves used in the filling procedure, which are named in the figure. The filling procedure consists of, first, filling the balance of the plant and the SunDials with valves E-13 and E-15 open, while the expansion tank is isolated with valve E-18. The air is vented by a valve located at the highest point of the installation, the connection line between the receivers. This is an automated valve that is controlled from the PLC. The automated vent valve will be open until HTF goes out through the valve, which means that there is no more air in the circuit. The main pump (MP) and recirculation pump (RP) have to turn on at minimal velocity to allow the flow to circulate through them to reach the SunDial.

The second step is the filling of the expansion tank, then valve E-15 is closed and E-18 is opened. The air of the tank is vented by E-11 while the HTF is being pumped in. The expansion tank requires to be filled over 25% of its capacity. Then, the vent valve E-11 is closed and the nitrogen is fed into the tank to pressurize to 1.5 barg. Finally, the tank is connected to the rest of the circuit opening valve E-15.

Hot commissioning: pre-heating and controller tuning

The main objectives of the hot commissioning are water elimination and the controllers' tuning. The water elimination is carried out by preheating the installation above 100 °C. The water is vaporized and vent from the automatic vent valve in the installation's highest point. After, the water is eliminated a series of tests can be performed to adjust the controllers' constants. The controller's constant where estimated with the dynamic model, thus, this value can be used as a first approach. However, in the real installation, this constant requires to be adjusted due to factors not considered in the simulation, which can produce delays in the response. For example, incrementing the gain constant could improve the response of the controller but will increase the instability of the control. A similar effect can be obtained by reducing the time constant.

4.2.3 Test procedures

The installation has been designed to conduct three sequential tests to evaluate the performance of the SunDials and the control strategy. The first test involves the preheating and defocus of the SunDial. This test will verify the control system's ability to manage temperature gradients during start-up and limit maximum temperatures, ensuring the safe operation of the system and preventing damage to the receiver. Following this, a performance test for the SunDial will estimate its peak power and efficiency. Finally, a control system test will be conducted to verify the proper implementation of the system's flexible heat demand strategy.

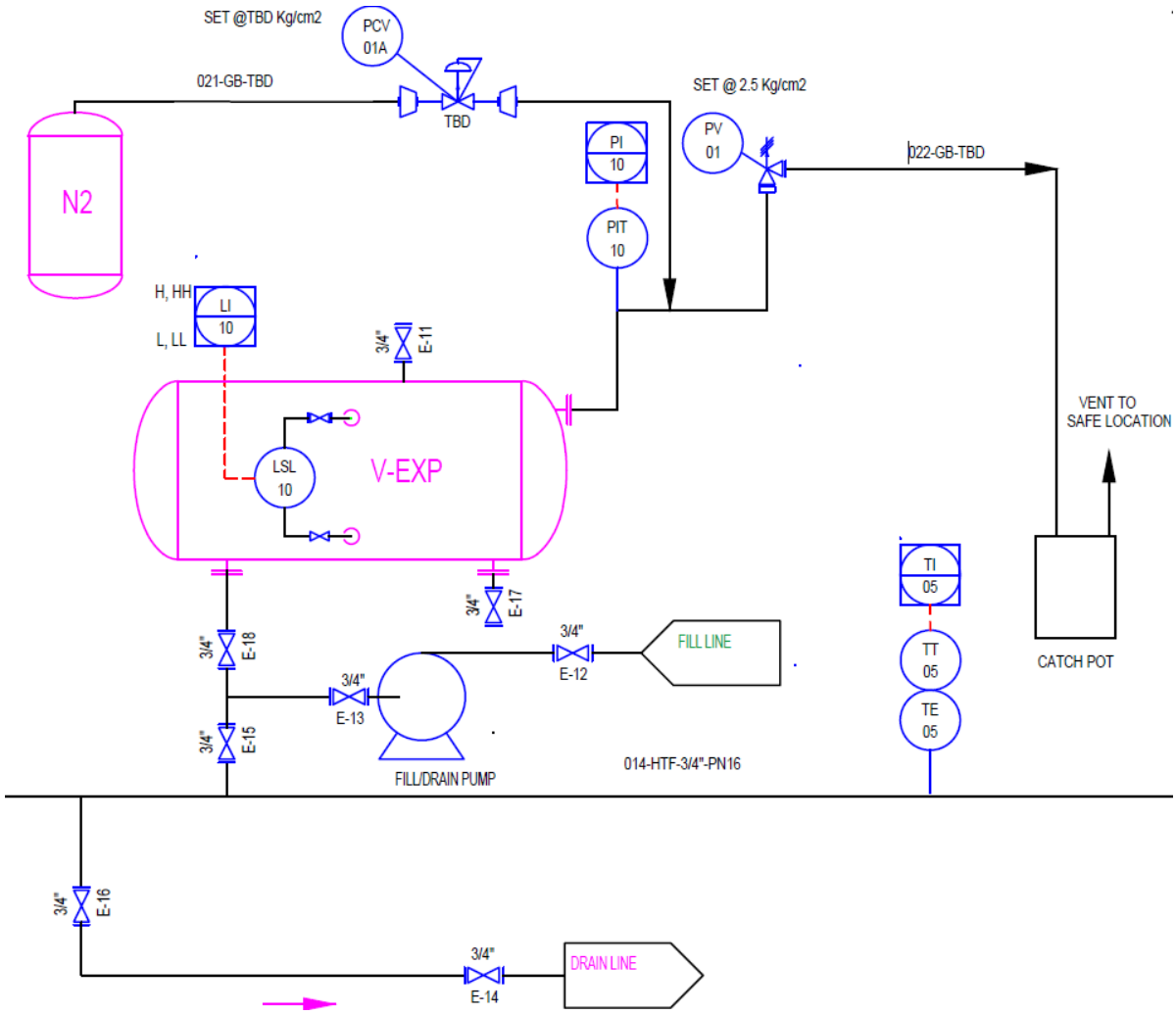

Figure 4.12: Expansion tank and main filling connection to the installation

Preheating and defocus test

The objective of this test is to evaluate whether the outlet temperature of the SunDial can reach the specified setpoints of 190, 205, and 220 °C, and to verify the performance of the defocus controller. One SunDial will be connected to the BOP and heated to achieve the first setpoint. The SunDial features a gradient temperature control that partially defocuses the solar collector to limit the maximum temperature gradient to 30 K/min. Maintaining this gradient is crucial to prevent damage to the receiver. The temperature will then be increased to the maximum to test the defocus controller.

The test can be performed by following the next steps:

1. Verify clear sky weather conditions.
2. Connect the SunDial to be tested and isolate the other one by closing one gate valve in the main manifold.
3. Ensure the FAN-demand cooler and the recirculation pump are turned off.
4. Fully open the bypass valve (BPV) in bypass mode so that there is no flow in the demand cooler.
5. Turn on the main pump (MP) and the SunDial recirculation pump (SP).
6. Start SunDial operation when the minimum DNI is reached.
7. Monitor the installation to ensure the gradient temperature control and defocus control function properly when the maximum temperature is achieved.
8. The experiment will be finished after the defocus controller operation is verified.
9. To end the experiment the SunDial is defocused completely, the MP is stopped, while SP works until the temperature of the SunDial decreases below 150 °.

After completing the test, the recorded data from the SCADA system will allow analysis of the controller's performance. The verification of maximum gradient temperature or maximum temperature is not exceeded is carried out. Additionally, thermal losses in the part of the system that has been tested can be determined by performing an energy balance once a steady state is achieved.

SunDial efficiency test

The objective of this test is to calculate the efficiency of the SunDia. This is calculated with Equation 4.8 and the measure data, which includes: the DNI, the mass flow rate, and the inlet and outlet temperature of the SunDial. The flow through the SunDial is constant, thus, the efficiency will depend on the DNI, and the inlet and outlet temperature of the SunDial. Other factors that influence the efficiency are the ambient temperature and the wind velocity but have a lower impact on the efficiency. However, these factors are also measured, thus, post-testing analysis can be carried out to evaluate their influence on the efficiency.

The DNI is a perturbation that can not be managed, but the inlet temperature of the SunDial can be controlled by the power extracted by the air coolers. The maximum power that the

two air coolers can extract operating simultaneously is 32 kW, this is higher than the peak efficiency of the SunDial. Therefore, the efficiency of the SunDial can be calculated at different outlet temperatures. For example, if the efficiency of the SunDials wants to be calculated at 215 °C, the inlet temperature of the SunDial has to be controlled to a different value depending on the power produced by the SunDial, as shown in Table 4.24.

It would be interesting to calculate the efficiency of the SunDial for the range of outlet operative temperatures, which goes between 190 and 240 °C. Therefore, if a step of 10 °C is selected 5 tests need to be performed. To carry out these tests clear sky conditions are required.

Table 4.24: Setpoint for the control inlet temperature fot the SunDial at different powers.

SunDial Power [kW]	Temp. difference [°C]	Outlet Temp. [°C]	Inlet Temp. [°C]
5	4.0	215	211.0
10	8.0	215	207.0
15	11.9	215	203.1
20	15.9	215	199.1
25	19.9	215	195.1

Control strategy test

The control strategy is designed to deliver heat to the factories by feeding the process at different temperatures and power levels for the tube steel factory and three for the dairy factory. For example, in the dairy factory, the three levels are 205 °C / 8 kW, 190 °C / 6 kW, and 220 °C and 14kW; in the tube steel factory the two levels are205 °C / 7kW and 220 °C /14 kW. The control strategy was previously explained in Section 4.1.3, and is performed automatically by the control system. During the test, all the components of the test ring are operative and the variables of Table 4.11 are recorded to calculate the KPIs in Table 4.2.1 .

It is interesting to perform the test with different DNI conditions, such as a clear sky and clouds so that the effectiveness of the control strategy can be fully evaluated. From the test results, it is important to check the demand inlet temperature control, the defocus controller, and the power extracted by the air-coolers. Especially to verify the automatic implementation of the different levels of power extract by the demand-cooler.

The data record with information about the performance of the actuators (pumps, valves, motors, etc) controlled by the control system can be used to analyze the system performance. The results of this test will be used to validate the dynamic model developed in Section 3.1 by the methodology explained in the next section.

4.3 Methodology for the dynamic model validation

The model validation process will involve conducting simulations using the weather data recorded during the experimental testing of the SunDials, the DNI, the wind velocity, and

the ambient temperature. Subsequently, the simulation results will be compared with the data obtained from the temperature and flow sensors placed at identical locations in both the model and the actual installation.

However, the SunDial model, in Chapter 3.1, needs to be modified to be able to receive as an input the DNI instead of the impinging power. In the SunDial model, the power absorbed by the receiver is calculated with Equation 4.14, where q_{conc} is an input to the model. Now, the impinging power to the receiver (q_{conc}) is calculated with Equation 4.15 which depends on the DNI, the reflective area (A_{ref}), and the incidence angle modifier (IAM).

$$q_{\text{abs}} = q_{\text{conc}} \cdot \eta \cdot d \tag{4.14}$$

$$q_{\text{conc}} = A_{\text{ref}} \cdot \text{DNI} \cdot \text{IAM} \tag{4.15}$$

For the IAM, a correlation with the zenith angle θ_z is estimated with the results of the Montecarlo ray-tracing simulation for the SunDial-HL in Romania and the SunDial-LL in Greece. In the case of SunDial-LL, the correlation is presented in Equations 4.16 and is plotted with the ray-tracing in Figure 4.13a .

$$\begin{aligned} IAM_{LL} &= 0.66, \theta_z < 33 \\ IAM_{LL} &= -0.0095 \cdot \theta_z + 0.968, 33 \leq \theta_z < 60 \\ IAM_{LL} &= -0.0166 \cdot \theta_z + 1.3783, 60 \leq \theta_z < 80 \\ IAM_{LL} &= 0.05739, \theta_z \geq 80 \end{aligned} \tag{4.16}$$

The SunDial-HL correlations (Eq. 4.17) are plotted in Figure 4.13b simultaneously with the ray-tracing model. It is evident that for zenith angles below 60°, deviations exist between the model and the correlations. These variations in the IAM value may be attributed to the receiver shadowing on the mirrors, which are independent of the cosine factor.

$$\begin{aligned} IAM_{HL} &= 0.6281, \theta_z < 60 \\ IAM_{HL} &= -0.0144 \cdot \theta_z + 1.493, \theta_z \geq 60 \end{aligned} \tag{4.17}$$

The IAM equations are included in the SunDial Model, thus, the inputs to the model are actualized to the DNI, zenith angle, ambient temperature, and wind velocity. To compare the results of the IAM correlation with the ray tracing model, two identical simulations for both inputs are carried out. The results show that the IAM correlation overestimated the energy produced by the SunDial. Figure 4.14 shows the energy of each component, where around 1% difference can be appreciated between the two models. The energy generated by SunDial-LL using correlation is 2.12 kWh more than ray-tracing simulation and for SunDial-HL it's 4.6 kWh higher.

The next steps will involve the calculation of the KPIs with the information that will be recorded in the experimental testing. Then, a comparison of the simulated values with the real

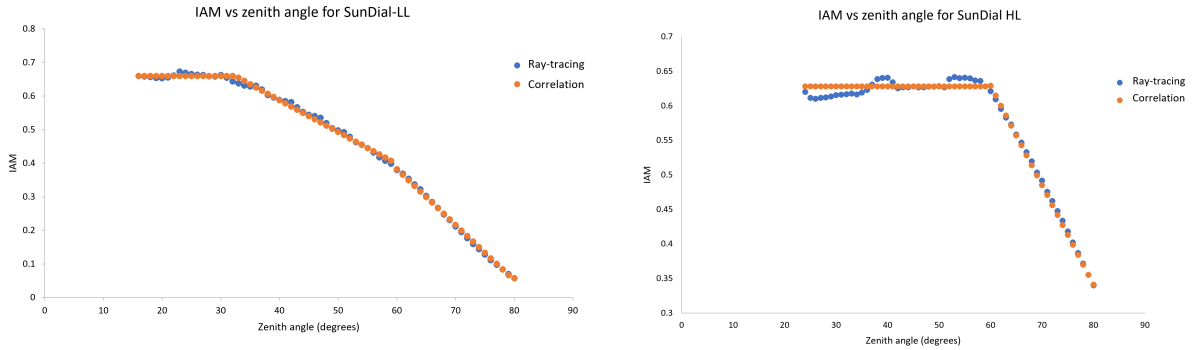

(a) **(b)**

Figure 4.13: IAM versus zenith angle ray-tracing and correlation for (a) SunDial-LL and (b) SunDial-HL

values will be carried out, including the power generated by the SunDial, the power extracted by the air coolers, the thermal losses, the preheating time, and the different temperatures reached in the system. With this information, the dynamic model will be adjusted to reflect the real thermal inertia of the installation, the residence time, the efficiency of the SunDial and air coolers, and the thermal losses.

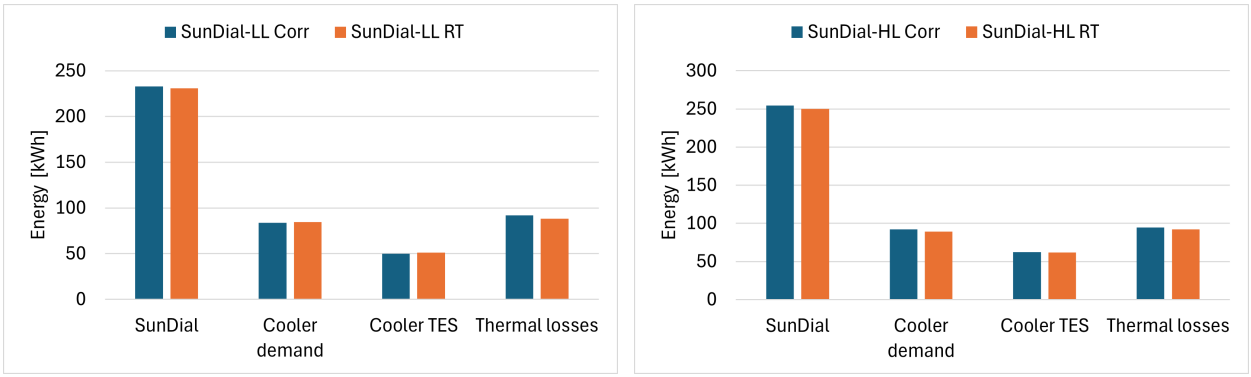

(a) **(b)**

Figure 4.14: Energy of the different components with the ray-tracing model and the correlation model.

4.4 Findings

The experimental installation, along with the SunDial collector and test facility, was constructed in Madrid using components sourced from local providers to minimize greenhouse gas emissions associated with transportation. This demonstrates that the SunDial collector can be assembled using readily available components from local markets, thereby supporting regional economies. Furthermore, the installation was designed for convenient packaging, disassembly, and transport to end-users.

The experimental facility requires two air coolers to replicate the end-user operation. The first air-cooler will work as the TES in charge mode. The latent thermal storage has an outlet temperature profile approximated by linear equations. These equations are used to control the extracted power by the air-cooler, by modifying the speed of the air-cooler fan with a PI controler.

The second air cooler is required to extract the heat sent to the demand. The cooler needs to be able to mimic the flexible heat strategy with different levels implemented in the end-users. Here, the control implemented is based on the temperature difference achieved in the cooler which is related to the power directly due to the HTF mass flow being constant.

The piping system was designed with a maximum pressure of 8 barg, which considers a safety factor of two over the operation pressure. The SunDial circuit counts with a pressure relief device that will be activated in case of a thermal expansion scenario.

Seven KPIs are defined to accomplish the two main objectives: the SunDials characterization and the testing of the control strategy. The maximum uncertainty calculated was for the SunDial efficiency with 3%, then an uncertainty of the power 1.1% was estimated. Three sequential tests are required to collect the information necessary to calculate these KPIs.

The balance of the plant is elevated one meter from the ground to be resilient to possible flooding. Due to delays in the construction of the installation caused by external factors, including two floods due to a river overflowing near the site, the testing plan to validate the dynamic model could not be completed before the presentation of this thesis. However, the validation methodology was presented, where an IAM correlation was included to the model developed in Chapter 3 to be able to perform simulations with DNI measure in the experimental site as an input to the model.

Chapter 5

Techno-Economic Analysis

This Section aims to undertake a techno-economic analysis of the SunDials and the ASTEP concept. Initially, the SunDial collector's cost analysis will be conducted, encompassing a detailed analysis of the materials and processes involved in the prototype construction at Tecnogetafe in Madrid, Spain. It is noteworthy that the cost of a prototype is notably higher than that of a commercial collector, primarily due to the absence of economies of scale. Subsequently, a scale-up analysis for the SunDial collector will be presented to estimate the final product cost.

Secondly, the economic viability of the ASTEP system is assessed by evaluating its Levelized Cost of Heat (LCOH), a technology-neutral metric. The LCOH is determined by dividing the overall system expenditure by the annual energy yield. To point out the key parameters influencing the LCOH, a sensitivity analysis is conducted. The objective of the sensitivity analysis is to find which variables have more impact on the LCOH. The outcomes of this analysis are used to look for enhancements to the ASTEP concept and to find an optimized solution to provide low-cost heat to the processes industry.

Finally, the SunDials will be compared with their primary competitor in the market, the PTC collector. Therefore, a dynamic model for the PTC was introduced in the ASTEP simulation and the performance of the two collectors was compared in terms of energy and LCOH.

5.1 Cost analysis for the SunDial

In the Concentrate Solar Power (CSP) sector, the installed cost has decreased by 64% between 2010 and 2020 [47]. A recent cost analysis for parabolic trough collectors (PTC) estimates a 120 USD/m^2 installation cost for solar collectors of aperture area 1576 m^2 and 803,760 m^2 of solar field used to power generation[54]. Other studies have been conducted for LFC, for example, Sait et al. [70] estimated 194.29 €/m^2 for a mirror area of 1750 m^2 per collector, and Ordoñez et al. [60] 153.81 €/m^2 for a mirrors area of 625 m^2 per collector. These studies share the common practice of breaking down collector costs into categories, as shown in Table 5.1. A comparison of these categories reveals that PTCs achieve a very low cost for the

receiver, which consists of an evacuated tube and support arms. The most expensive category for PTCs is the structure, which compromises the space frame, support arms and foundations. The LFC collector exhibits a lower cost for the structure but a higher cost for the mirrors and tracking category. The LFC receivers costs shown in Table 5.1 are higher than the PTC receiver cost due to the use of a multi-tube with a trapezoidal secondary reflector type, which is not a standard component like the evacuated tube.

Table 5.1: Cost for large solar concentrators for power production.

Cost €/m^2	LFC Sait 2015 [70]	LFC Ordoñez 2023 [60]	PTC Kurup 2022 [52]
Structure	57.14	31.3	63.1
Mirrors and tracking	57.14	61.0	36.6
Receiver	68.57	52.4	16.3
Piping	11.43	9.11	4.00
Total	194.29	153.81	120.00

The cost of solar collectors applied to SHIP has not achieved such a low value as the CSP for electricity generation. The main difference between these collectors is the size, being the ones used for the industry sector smaller. This difference in size is primarily due to the characteristics of the industry demand, contrary to electric generation, which requires higher temperatures and larger capacities. The needs for the industry application as follow: capacity between 1-1000 MWh/y, temperatures range between 100 and 400 °C, and limited space for the solar field. However, in the last 6 years, the cost of solar heat applied to industrial processes (SHIP) has decreased by 68% in Europe, from 1678 USD/kW to 531 USD/kW of total installed cost [32].

Obtaining short payback periods (lower than 3 years) is the most important factor to the industry sector, and this is highly dependent on several factors, such as the price of fossil fuels, the available DNI, and local taxes. A cost analysis carried out for SHIP projects in California in the United States concluded that the installation cost for the solar field must be reduced to values between 150 and 200 USD/m^2 to be attractive to the industry with a gas price of 23.4 USD/MWh and a production based incentive of 34 USD/MWh for 2 years [53]. Similar results have been found in a study carried out for LFC, where a price of 150 €/m^2 is required for DNI larger than 1900 kWh/m^{2}yr, a low cost of the gas between 30-50 €/MWh, and no subsidy [36]. In a study implementing flexible heat integration (FHI), the researchers compared the results with the gas prices of 23 USD/MWh. They found that for FHI, a cost of the solar field of 275 USD/m^2 will be competitive, while for a standard integration, the cost required is restricted to values lower 255 USD/m^2 [46].

The LFC is generally a more economical collector than the PTC, but its optical efficiency is lower. It has been found that the cost of the LFC has to be up to 70% of the PTC cost to be financially viable. Therefore, if the cost of the PTC is around 275 €/m^2 the LFC cost is required to be lower than 185 €/m^2 to compete with the PTC and also achieve a 3-year payback period. This was calculated in a research study for Greece's climate, with a heat production cost of 100 €/MWh which is a reasonable price in that region [13].

Other researchers have looked for a reduction in cost and higher efficiency for small LFCs specially designed for SHIP applications. For example, a novel Fresnel design by Plataforma Solar de Almeria achieves better energy results per land than a PTC. It shows lower LCOH when prices of land are over 60 €/m^2 for a cost of the solar field of 250-370 €/m^2 for the LFC and 500 €/m^2 for the PTC [15].

5.1.1 Prototype cost calculation

The SunDial was designed with the primary objective of achieving low cost, easy operation, and low maintenance. Figure 5.1 depict the two prototypes including the rotating paths and the HTF piping connections. The rotating paths were built for two reasons: first, the SunDial requires an even ground so that the wheels can move freely; second, the connection between the piping above the platform and the balance of the plant on the ground needs to go below the platform. In the location where the SunDials were built no civil works can be done so the piping can not be underground, thus, the rotating paths were the solution.

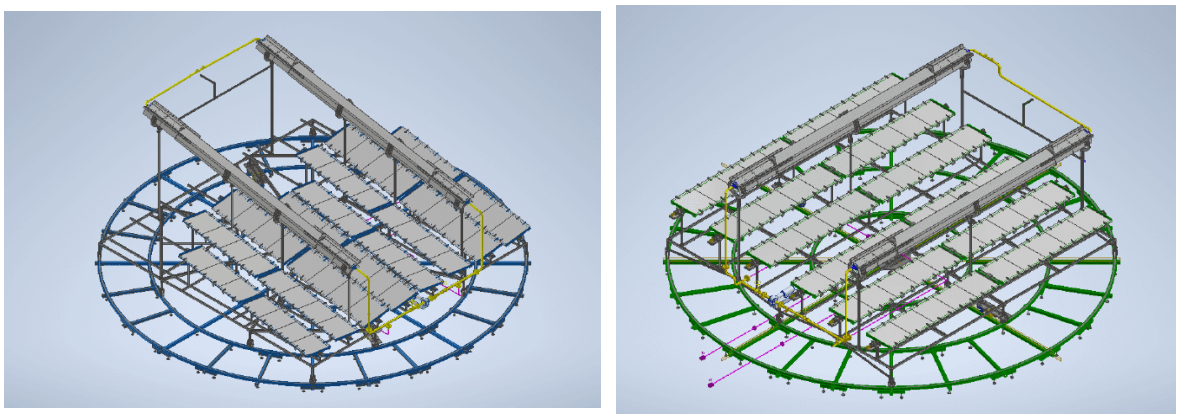

(a) **(b)**

Figure 5.1: (a) SunDial-LL and (b) SunDial-HL [7]

The Sundial prototype cost was calculated by considering the unitary cost of all the components bought in the ASTEP project to build the two prototypes in Madrid. Table 5.2 shows the cost of the two prototypes for the next categories: the platform structure including the wheels, the mirrors, and the structure to support them, the tracking which involves the motors and actuators, the receiver, the HTF components as piping and the thermal oil, the rails where the wheels rotate, and the labor and transport cost.

Figure 5.2 depicts the cost of each category per reflective area and average power, which is 22 kW for Corinth and 18 kW for Iasi. This was calculated by multiplying the reflecting area, 44 m^2, and the average DNI, 417 W/m^2 in Iasi; and 47.5 m^2 and 464 W/m^2 in Corinth. The main cost corresponds to the labour, since prototypes involve more working hours due to the first-time making, redoing, and supervision of the main researchers. The HTF category considers the cost of the recirculation pump of the SunDial and the insulation of the interconnection pipes.

Upon comparing the two prototypes, it is noticed that the tracking component is in the third position on the SunDial-HL while the SunDial-LL is the last. This is because the SunDial-HL counts with one additional motor per mirror. It is worth noting that the cost of the mirrors and the structure are comparable to the cost of the literature review. The main cost optimization of the SunDial is in the mirror-bending method and the structure [18].

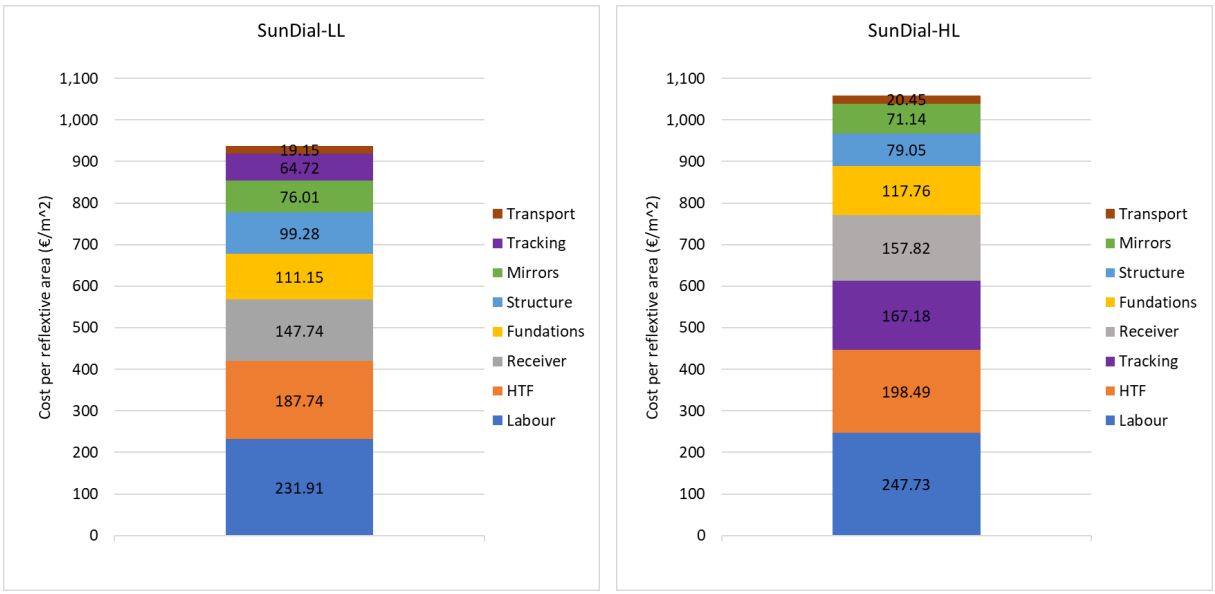

(a) **(b)**

Figure 5.2: Prototypes cost per reflective area for (a) SunDial-LL and (b) SunDial-HL

Table 5.2: Cost of the SunDial Prototypes per reflective area and average power

Element	SunDial-LL			SunDial-HL		
	€	€/m2	€/kW	Euros	€/m2	€/kWh
Structure	4,666	99.28	212.1	3,478	79.05	193.2
Mirrors	3,572	76.01	162.4	3,130	71.14	173.9
Tracking	3,042	64.72	138.3	7,386	167.9	410.3
Receiver	6,944	147.7	315.6	6,944	157.8	385.8
HTF	10,823	230.3	492.0	10,733	243.9	596.3
Rotating Paths	5,224	111.2	237.5	5,181	117.8	287.9
Labour	10,900	231.9	495.5	10,900	247.7	605.6
Transport	900	19.15	40.91	900	20.45	50.0
Total SunDial	46,072	980.2	2,094	48,653	1,105	2,703

A deeper analysis of the cost of the prototypes is performed by a Pareto graph of the specific components. The SunDials can be discretized in more than a hundred subelements, but only the 20 first elements are responsible for most of the cost. Figure 5.3 illustrated the expensive components of the SunDial prototypes, where the receiver is the first item, significantly higher than the rest. It is interesting to note, that several items correspond to the SunDial recirculation: the pump, the gate valves, the pipings, and the piping insulation.

The elements associated with the tracking system, primarily in the SunDial-HL, are presented between the expensive components. The gearboxes are positioned in the third position in both SunDials, also the motors and frequency drivers are included in the list. Motors used for solar tracking are required to move the collectors at a slow pace. Hence, the motor is mated to a gearbox which reduces the speed of the output shaft and increases the torque. The mate motor-gearbox provides the driving force to the actuators of the platform with a motor power of 180 W and a gear reduction of 2300:1. In SunDial-HL each line of mirrors counts with a motor of 50 W and a gear reduction of 100:1.

At the secondary level, several items associated with the rails manufacturing are presented in the Pareto graph. Also, the rotary joints appeared between the expensive components. These are required in the connection between the moving pipes above the platform and the static pipes of the balance of the plant. In the next section, an investigation of how the cost of the prototypes can be driven down by economies of scale is carried out.

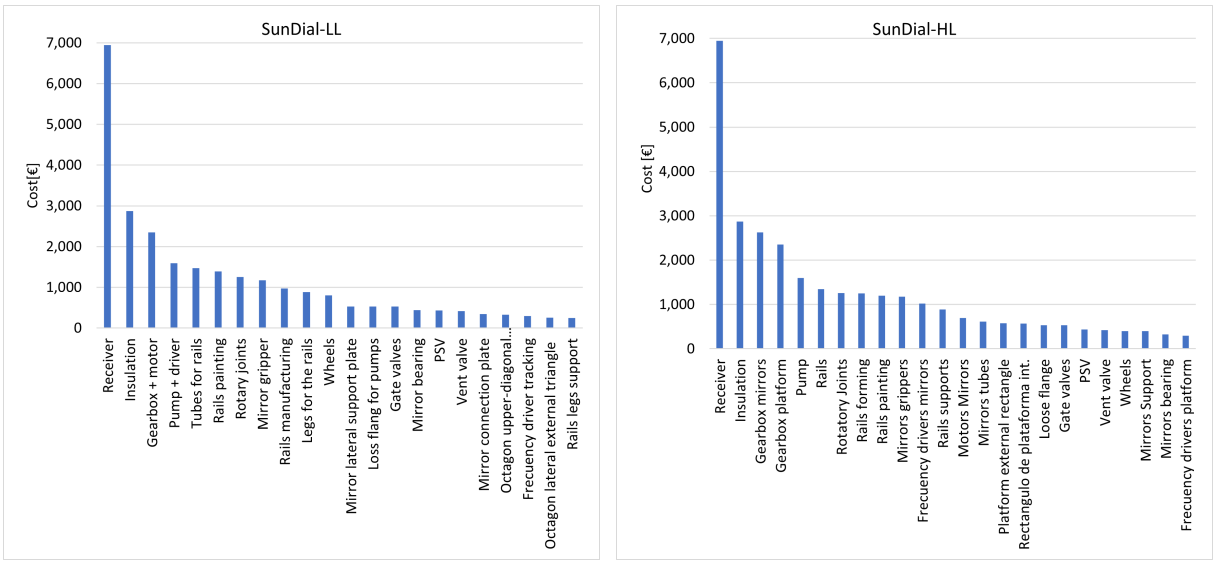

(a) **(b)**

Figure 5.3: Pareto analysis for the prototypes: (a) SunDial-LL and (b) SunDial-HL

5.1.2 Scale-up production analysis for driving down the SunDial cost

The prototype costs are higher than commercial technologies due to the hand-craft process which implies more labor hours, re-manufacturing, extra material, and lack of optimization. Furthermore, the cost of the components is highly reduced when buying more units than one or two. In the construction of the SunDial prototype, the material was bought in batches as the construction was progressing, and a total of three years of construction was required. For example, the cost of piping tubes and flanges was reduced by 50 % when buying more than 10 items.

Some over-costs in the construction of the SunDial are related to the lack of purchasing and logistic strategy. All the components have been bought from Spain due to the shorter shipping time, but a cost reduction can be obtained by importing the elements from other countries. For example, the cost of the motors and the rotating joints, which were bought by a local provider, can be reduced by purchasing directly from manufacturers.

Other cost optimization can be done by modifications in the prototype design. For example, the rails can be replaced by civil works, which can be cheaper depending on the characteristics of the location. Then, the receiver used was expensive, and a huge cost reduction can be done by using a standard evacuated tube. Finally, the recirculation of the SunDial can be eliminated by increasing the mass flow rate of the main pump. In the experimental installation, the balance of the plant was prepared for a small flow so the recycle pump was required. Furthermore, these elements are usually not considered in the cost of the solar collector, but instead in the cost of the BOP because are dependent on the application. Therefore, a more accurate price for the SunDial cost was calculated by taking the considerations resumed in Table 5.3.

Table 5.3: Considerations for the cost calculation for the SunDial scale production

Item	Lower	Upper	Comment
Receiver [€/m2]	36	52	data from literature[52], [60]
Steel square tube galvanized [€/kg]	1.575	2.4	40% price reduction based on market prices for the lower boundary
Laser-cutting steel pieces [€/kg]	2	4	50% price reduction based on the market price for the lower boundary
Laser-cutting Aluminium [€/kg]	12	24	50% price reduction based on the market price for the lower boundary
Piping and accessories	0.5	1	elimination of the pumping elements and a 50% price reduction based on the market price in the lower boundary
Components	0.45	0.5	price reduction for motors, gearboxes, and rotatory joints based on market price in upper and lower boundaries
Labour	1 weeks	2 weeks	two workers, laubor cost per hour in Spain is 20 €/h [20]

An upper and lower boundaries of the SunDials cost have been obtained using the considerations shown in Table 5.3. As depicted in Figure 5.4, the cost per square meter of reflective area for the SunDial-LL is between 215.2 and 320.8 €/m^2, and for the SunDial-HL is 234.6 -348.5 €/m^2, which is lower than the actual cost of 400 €/m^2 in Europe. However, the target found in the literature review of 200-150 €/m^2 has not been reached.

Upon comparing the costs obtained from the SunDial estimation and the ones outlined in Table 5.1, it becomes evident that the SunDial-HL tracking system incurs significantly higher expenses. This discrepancy arises from the fact that each line of mirrors is equipped with its

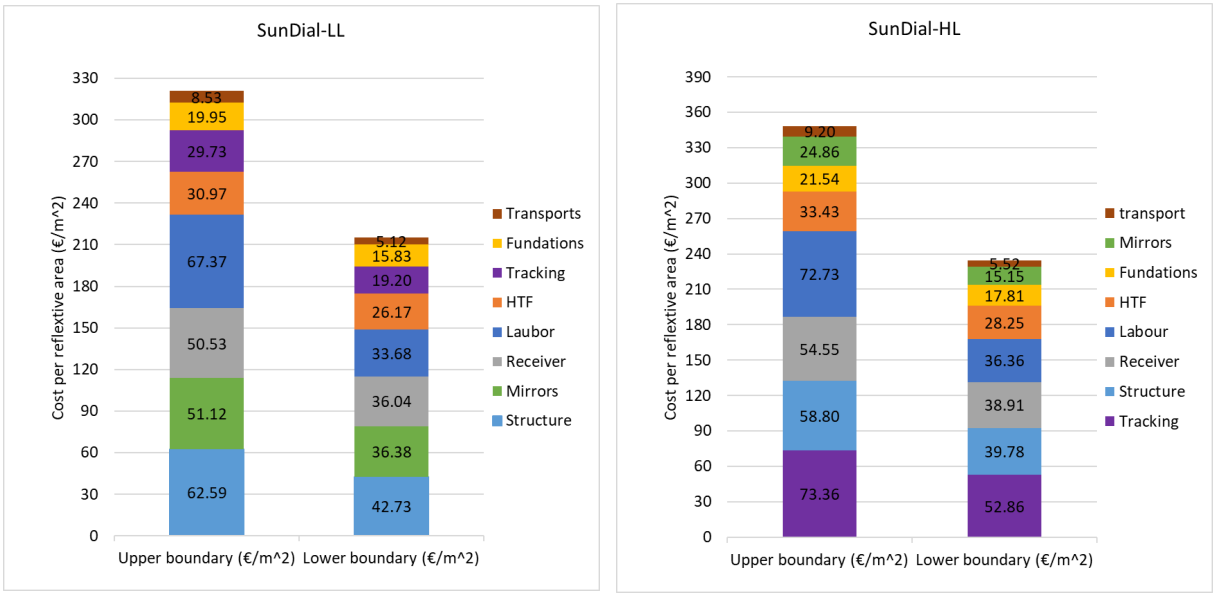

(a) **(b)**

Figure 5.4: Upper and Lower boundary for the cost per reflective area: (a) SunDial-LL and (b) SunDial-HL

motor, and these mirror lines are relatively small compared to those in larger collectors. If the mirrors were extended, the same numer of motors would still be necessary, but the collector's area would increase, leading to a reduction in cost per unit area. The same principle applies to the rotating joints. However, there is a point where increasing the SunDial size will not represent a cost reduction. Consequently, an inquiry into determining the optimal size of the SunDial collector to minimize costs is performed in the next section.

5.1.3 Optimizing the SunDial size

The size of the SunDial collector can be increased by extending the platform to obtain cost reduction due to the optimization of materials in the collector construction. The benefit of doing this is to optimize the most expensive materials, the motors, gearboxes, and rotatory joints by applying the same number of elements to a larger reflective area. The platform can be extended by increasing the length of the receivers and mirrors or by adding parallel mirrors and receivers above one platform.

The SunDial is designed to be over a square platform. The evacuated tubes that are used in the receiver are produced in a standard length of 4 m. The SunDial has two of these tubes connected in series, giving the receiver a total length of 8 m. Each receiver has associated three lines of mirrors. The SunDial platform has two receivers installed in parallel lines (but connected in series), summarizing a total of 6 lines of mirrors per platform. Therefore, the SunDial square platform can only be a multiple of 4 if a standard evacuate tube is used. The immediate standard sizes of platforms are 12x12, 16x16, 20x20 and 24x24. The three first sizes are depicted in Figure 5.5 to have a visual representation of how the larger platforms

will be built. Then, the principal parameters of each design are shown in Table 5.4.

The SunDial 12x12 was built by connecting three evacuated tubes in series to form a receiver of a total length of 12 m, and three receivers in parallel to form a 12x12 platform. Each receiver has three associated lines of mirrors. The SunDial 12x12, will maintain the same tilt as the SunDial 8x8 so that the efficiency of the collector will not be affected. This means that the higher point of the receiver will be increased to 2.9 m for the SunDial-HL and to 4.1 m for SunDial-LL. The total reflective area of this platform is 99 m^2.

The SunDial 16x16 can be built by connecting 4 parallel receivers of 16 meters or 2 parallel receivers of 32 meters. The total reflecting area of this collector is equal to 4 SunDial platforms, e.i. 176 m^2. However, the SunDial 16x16 presents some advantages, such as lower land occupancy and fewer interconnecting pipes compared to 4 SunDials 8x8. The principal disadvantage is that the higher point of the receiver will be increased to 3.4 m in SunDial-HL and to 4.8 m in SunDial-LL.

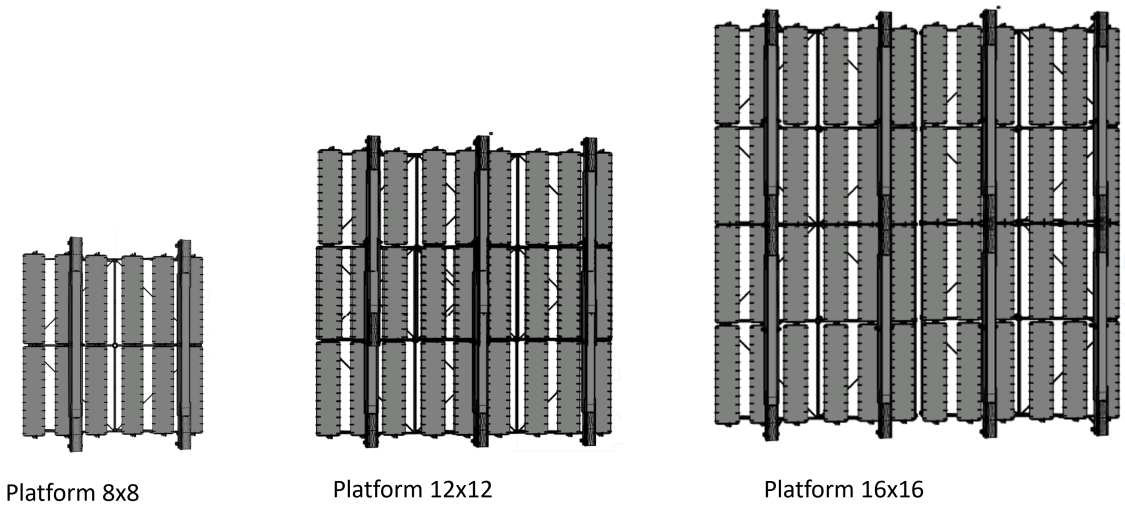

Figure 5.5: SunDial-HL in three different sizes.

Table 5.4: Principal parameters of the SunDial in different sizes

Platform size	Reflecting area [m^2]		Total land [m^2]		Peak Power [kW]	
SunDial	HL	LL	HL	LL	HL	LL
8x8	44.0	47.5	103.1	116.2	18.3	22.0
12x12	99.0	106.9	232.0	261.5	41.3	49.6
16x16	176.0	190.0	412.4	464.8	73.4	88.2
20x20	275	296.9	400	430.5	114.3	137.5

A cost analysis was performed to find which is the optimum size of the SunDial. The method used to calculate the cost of the larger versions of the SunnDial is described in Appendix D. Figure 5.6 depicts the lower and upper boundaries for the different sizes of the SunDials. The SunDial- LL achieves the optimum value for the sizes 12x12 for a cost between 184.5 and

270 €/m^2. The increment in the cost of the SunDial-LL 20x20 is due to the collector's higher point being increased to 7 meters to maintain the 10-degree inclination of the mirrors and the receiver.

The SunDial -HL achieves the optimum cost for the 16x16 size with a value between 169.5 and 265 €/m^2 and this cost range is maintained constant for the larger versions. The main factor in the cost reduction of this collector is the tracking category due to the length of the mirrors being extended so the cost of the motors and gearboxes per area is reduced.

It is interesting to notice, that the total price for the SunDial-HL is lower than the SunDial-LL in the larger versions due to a high-cost reduction in the tracking system for the SunDial-HL and a higher increase in the categories of mirrors and structure in the SunDial-LL. This cost inversion for the SunDial-HL platform is due to the lighter structure and the lower tilt in comparison to the SunDial-LL. In the SunDial-LL, the cost for the structure is increased from an average of 53 €/m^2 in the SunDial 8x8 to 106 €/m^2 in the SunDial 20x20, while for the SunDial-HL the same category presents a lower increase from 49 to 69 €/m^2. Similar behavior is observed in the mirrors category, which goes from 44 to 90 €/m2 for the SunDial 1-axis and 20 to 28 €/m^2. This means that the SunDial-HL in the larger version will be more cost-competitive also at low latitudes than the SunDial-LL.

The prices of the different categories are now comparable with the ones of large collectors from the literature shown in Table 5.1. As a result, the total cost per reflective area of the collectors has been reduced and fits in the target found in the literature review of 200-150 €/m^2 to be competitive with the actual competitors, the fossil fuels.

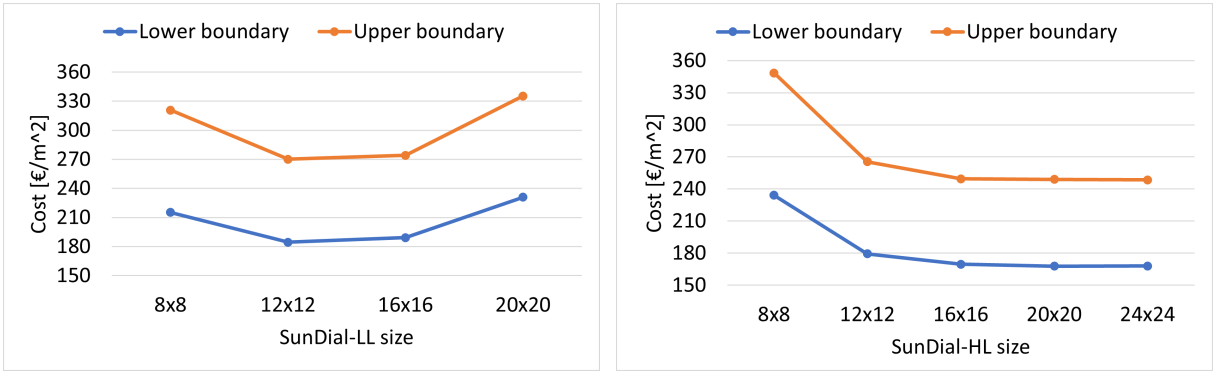

(a) **(b)**

Figure 5.6: Cost per reflective area for the upper and lower boundaries vs the SunDial size (a) SunDial-LL and (b) SunDial-HL

To summarize, it was found that SunDial collectors can achieve competitive prices in the industry through the reduction of cost from the prototype by economies of scale. Furthermore, larger versions of the original SunDials were designed to achieve an even lower cost by an optimization of the expensive elements per reflective area, which were the tracking motor-gear mate and the rotary joints. The main finding was that for the larger sizes of the SunDial, the 2 tracking axes version (SunDial-HL) is cheaper than the SunDial with one axis (SunDial-LL). This implies that in the low latitudes locations will be convenient to apply the SunDial with

2 tracking axes due to its lower price and high efficiency. However, the price of the heat is dependent on more factors, including the location. Therefore, in Section 5.2, the factors that affect the levelized cost of heat (LCOH) are investigated.

5.2 ASTEP performance and sensitivity analysis

It was found that the targets of annual energy production were not achieved with the ASTEP system due to the higher thermal losses due to the small size of the SunDial. In this section, other configurations for ASTEP, including the enlarged versions of the SunDials, were explored by using the annual model explained in Section 3.3. The main objective is to find the main variables of the ASTEP system that influence the LCOH. Then, this information is used to design the ASTEP system with the lowest value.

The LCOH was calculated with Equation 5.1. Here, I_0 is the investment expenditure at year zero, M_t is the operation and maintenance expenditure per year, Y_t is the annual heat generation, r is the discount rate, the subfix t is the number of years, and n is the project's lifetime.

$$LCOH = \frac{I_0 + \sum_{t=1}^{n} \frac{M_t}{(1+r)^t}}{\sum_{t=1}^{n} \frac{Y_t}{(1+r)^t}} \tag{5.1}$$

The objective of this study is to find which variables of the ASTEP system have more impact on the levelised cost of heat (LCOH). By identifying these variables the ASTEP system can be optimized to achieve the lowest LCOH. In a sensitivity analysis, the LCOH is calculated for each single value of the variable in the selected range maintaining the rest of the variables in the base case. The variables range and the base case are shown in Table 5.5. For example, the LCOH is calculated for a cost of the SunDial of 150, 180, 220, 240, and 260 €/m^2, and the rest of the variables shown in Table 2 were maintained at the base case scenario.

The selected variables can be divided into cost variables such as the SunDial, the TES, the BOP, and the maintenance and operation (M&O) cost; financial variables such as the discount rate; and system variables such as the TES capacity, the SunDial size, the defocus temperature, and the solar multiple. The SunDial and the BOP cost range were selected taking into account the cost estimation carried out in Section 5.1.2 and the values found in the literature research presented in Section 5.1. The TES range of cost was taken from the techno-economic report carried out by IEA [45]. The M&O costs are estimated to be 0.5 % of the total installed cost per year for large solar fields (>1000 m^2) and 1 % for small fields [32], so the range was set to 0.25 to 1 %. The discount rate has varied between 3.5 % and 7 %, and the base case was set to 5 %, which is the value recommended by the solar payback project [32] .

Regarding the system variables, the TES number of modules connected in parallel was increased from 0 to 5 modules. The defocus temperature was limited between the maximum

temperature admitted for the thermal oil degradation, which was 290 °C, and the process temperature which was 220 °C. Increasing the defocus temperature implies increasing the storage model capacity, for an increase from 240°C to 290°C the energy stored per module increased from 57.2 to 89.2 kWh. Finally, the total power demand by the process was varied to the next values: 10, 14, 24, and 34 kW.

SunDial 12x12 was selected as the base case and the SunDial 8x8 and SunDial 16x16 were used as lower and upper range. To simulate the SunDial 12x12, the SunDial 8x8 model explained in Section 3.1.2 was modified. The model utilized the same two Modelica standard pipes to simulate the receiver but one of them is 8 meters in length while the second of 4 meters. Then, the second pipe will receive 50 % of the power concentrated by the first. Three of these two-pipe arrangements will be connected in parallel. The ASTEP system for the SunDial 12x12 platform size will be identical to the original SunDial but with an increase in the SunDial, recirculation pump mass flow rate to 9 kg/s, to maintain the velocity over 1 m/s. The SunDial 16x16 with two parallel receivers of 32 meters was modeled by connecting two SunDial 8x8 models in series and two sets of the series assembly in parallel. The SunDial pump recycle mass flow rate is set to 6 kg/s.

If the size of the solar field is increased without changing the power fed to the process then the solar multiple of the system will change. The solar multiple is an important parameter of a system and is calculated as the ratio between the solar field thermal power and the process thermal power. The SunDial average power is 22 kW for Corinth and 18 kW for Iasi, which is calculated by multiplying the reflecting area, 44 m^2, and the average DNI, 417 W/m^2 in Iasi; and 47.5 m^2 and 464 W/m^2 in Corinth. The thermal power fed to the process is 14 kW, so the solar multiple is 1.57 in Corinth and 1.28 in Iasi. The TES consists of 2 modules connected in parallel, which can store a total energy of 57.2 kWh per module between the range of temperatures 190 and 240°C.

The simulations were done by fixing the solar multiple to the base case, which is the SunDial 12x12 with a demand of 14 kW. Thus, the demand applied to SunDial 8x8 was 7 kW and to SunDial 16x16 was 24 kW. The SunDial cost used to calculate the initial investment (I_0) was the average between the upper and the lower boundary estimation for each collector in Section 5.1.3 . The elements of the balance of the plant are the same despite the collector size. Hence, if the size of the SunDial increases, the cost of the BOP per reflective area is reduced. The result is a BOP cost for SunDial 12x12 of 40 €/m^2, then for SunDial 8x8 80 €/m^2 and for SunDial 16x16 20 €/m^2.

If the demand power is increased while the flow through the heat exchanger (HX) remains constant, the temperature difference must increase. In the dairy factory, the inlet to the second heat exchanger is regulated using a bypass and a recirculation pump. Therefore, it is crucial to maintain the outlet temperature of the first HX at the base scenario level (190 °C). To achieve this, the demand flow needs to be adjusted accordingly: 0.16 kg/s for 10 kW, 0.39 kg/s for 14 kW, and 0.55 kg/s for 34 kW. This same procedure is applied in the SunDial 16x16 scenario, where the demand was increased to 27 kW to match the solar multiple of the base case. Consequently, the demand flow was set to 0.45 kg/s to maintain the temperature difference in the HX.

Table 5.5: Sensitivity analysis variables base case and range of variation.

Parameter	Value	Range
SunDial cost (€/m^2)	SunDial-HL=220, SunDial-LL=227	180,200,220,240,270
TES cost (€/kWh)	30	10,20,30,40,50
BOP (€/m^2)	40	10,20,40,60,80
M&O cost (%)	0.5	0.25,0.5,1
Discount rate (%)	5	3.5,5,7
TES number of modules	2	0,1,2,3,4,5
SunDial size	12x12	8x8,12x12,16x16
Temperature operative range (°C)	190-240	190-230,190-240,190-290
Demand (kW)	14	10,14,25,34

5.2.1 Cost uncertainty analysis

This section focuses on cost uncertainty. The results related to cost and financial parameters are illustrated in Figure 5.8, showing the levelized cost of heat (LCOH) and the percentage variation of selected variables. A decrease from the base case is represented as a negative percentage. The results indicate that the cost of the SunDial and the discount rate are particularly sensitive variables, as evidenced by their pronounced slopes. Specifically, a 20 % reduction in SunDial cost results in a 15% reduction in LCOH in SunDial-LL and 20 % in SunDial-HL, while a 30 % reduction in the discount rate leads to a 12 % reduction in LCOH.

The variables with less effect on the LCOH were the O&M cost, the TES cost, and the BOP cost. The reason for this is that the cost of the BOP and the TES is one order of magnitude lower than the SunDial so the impact in the LCOH is lower. The cost for M&O is also low in comparison with the initial investment. A reduction of 50 % on the O&M cost only represents 3 % in the LCOH. The TES cost and the BOP cost present similar results, for a 60 % reduction a 9 % reduction of the LCOH is obtained.

The base case for SunDial-HL results in a lower LCOH than the SunDial-LL. This is because the SunDial-HL 12x12 has a lower average cost per area and the energy produced is similar.

5.2.2 ASTEP system sensitivity analysis

The results for the system variables are illustrated in Figure 5.8 , where it is evident that the SunDial size, the demand power, and the defocus temperature are variables with high influence in the LCOH. The SunDial 8x8 implies a 40 % increase in the LCOH, and the SunDial 16x16 has a reduction of 42 % for the SunDial-HL and 28 % for the SunDial-LL. The demand increased to 34 kW, which means a reduction of the solar multiple to 1.4 from 3.7, presenting a decrease of the LCOH of 42 %. However, a reduction of the solar multiple implies a lower manageability. For the defocus temperature, a 100 % increase in the temperature

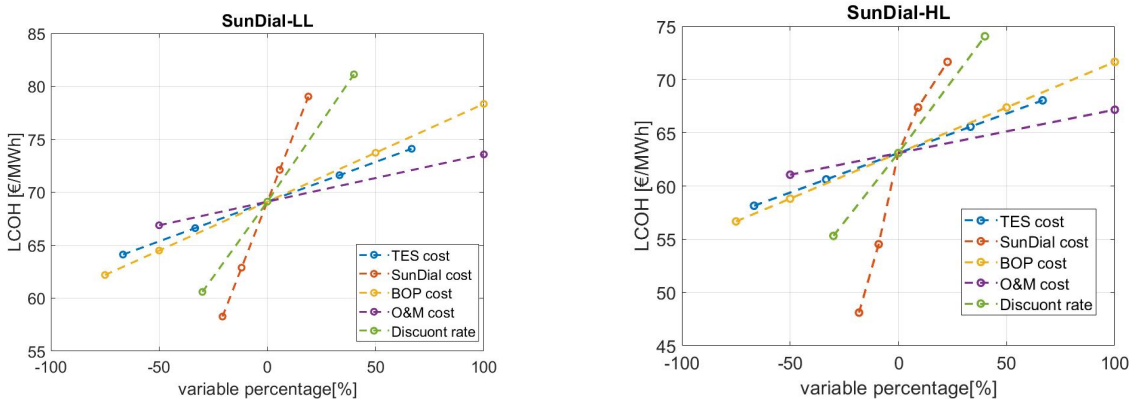

(a) **(b)**

Figure 5.7: LCOH cost uncertainty results for the SunDial-LL (a) and SunDial-HL (b)

operation range (190 to 290 °C) represents a 14% LCOH decrease.

The lowest LCOH achieved for the SunDial-HL is 40 €/MWh for the higher demand power, so the lower solar multiple and the SunDial 16x16. Furthermore, the LCOH can be reduced by combining all the variables that reduced the LCOH, which are increasing the defocus temperature to 290 °C and using the SunDial 16x16 with a solar multiple of 1.4, this will be done next.

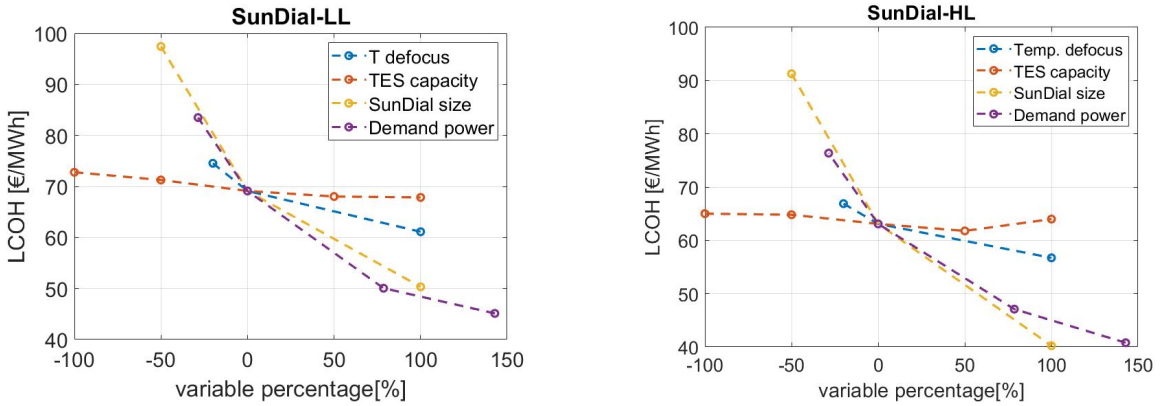

(a) **(b)**

Figure 5.8: LCOH sensitivity results for the SunDial-LL (a) and SunDial-HL (b).

For the SunDial-LL, the lowest LCOH is also achieved for the higher power demand and is 45 €/MWh, higher than the SunDial-HL. As in the SunDial-HL, a further decrease of LCOH can be expected for a simulation with the SunDial 16, a defocus temperature of 290 °C, and a solar multiple of 1.4.

The number of TES modules seems not to have a great impact on the LCOH cost. In terms of lower LCOH, the optimum number is 4 modules. But to better understand the optimal number of modules, the solar fraction of the system is evaluated. The solar fraction has been calculated as the ratio of the total energy supply by SunDial and the nominal demand, which

is 75.92 kWh in the dairy factory and 122.64 kWh in the tube steel factory. The demand is higher in the tube steel factory due to the operation 24/7 while in the dairy factory, the boiler is working only between 8 am and 5 pm. Figure 5.9 shows the evolution of the solar fraction with the number of modules for the two systems. From this figure, it is seen that the solar fraction increases with the number of modules until four, where the increase is small in the case of SunDial -LL and null in SunDial-HL.

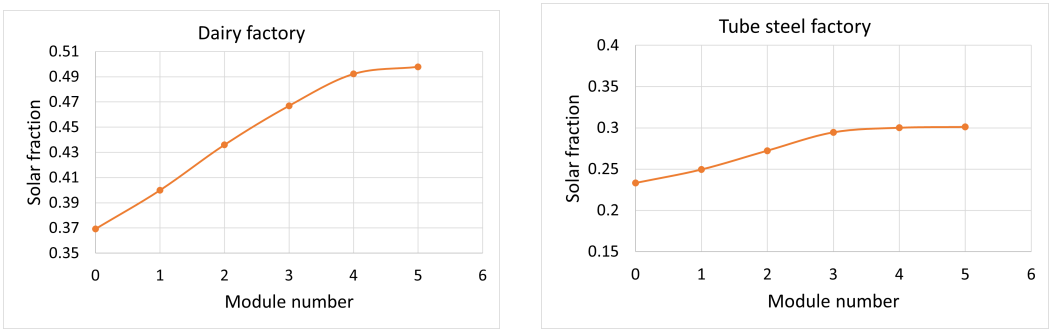

(a) **(b)**

Figure 5.9: Solar Fraction versus the number of modules SunDial-LL (a) and SunDial-HL (b).

The simulation for the optimal case found with the sensitivity analysis of the SunDial 16, with a defocus temperature of 290 °C, 2 storage modules, and a solar multiple of 1.4 was performed for the SunDial-HL and SunDial-LL. Regarding the LCOH, the results in Table 5.6 show a lower value than the actual cost of natural gas in Europe of 33 €/MWh [82], which means that this technology could be competitive with fossil fuels.

Table 5.6: Results for the annual simulation of the optimal case

Parameters	SunDial-HL	SunDial-LL
Process Energy [MWh/y]	100.7	93.8
η_{Sun} [%]	77.0	78.5
η_{Pro} [%]	68.2	62.4
TL [%]	11.5	14
Reflective area [m^2]	176	190
LCOH [€/MWh]	26.4-36.54	32.9-44.6
Cost SunDial [€/m^2]	170-250	190-270
Defocus [°C]	290	290
SM	1.4	1.4

In summary, it was determined that the key variables influencing the LCOH include the cost of the solar collector, solar multiple, SunDial size, and defocus temperature. The cost of the solar collector is closely tied to its size, benefiting from cost reductions due to economies of scale, such as those derived from fixed costs like the tracking system or rotary joints, which remain constant for larger collectors. Lower solar multiples contribute to decreasing LCOH and increase the efficiency of the solar field. Moreover, maximizing the defocus temperature, or the maximum store temperature, is essential for achieving higher efficiency and lower

LCOH. Ultimately, the optimized scenario resulted in a lower LCOH than the prevailing natural gas price in Europe, which stands at 33 €/MWh in both locations: 26.4 €/MWh in Iasi, Romania, and 32.9 €/MWh in Corinth, Greece. For instance, in central Europe, the gas price has remained stable at 33 €/MWh over the past year, as depicted in Figure 5.10.

The main finding is that the cost of the LCOH decreased using the larger versions of the SunDial. This means that it will be convenient to use the SunDial with two tracking axes (SunDial-HL) also for the low-latitude locations to achieve a lower LCOH. In the next section, the SunDial with 2 axes will be implemented in the low latitude location and will be compared with the main competitor in the market the PTC collector.

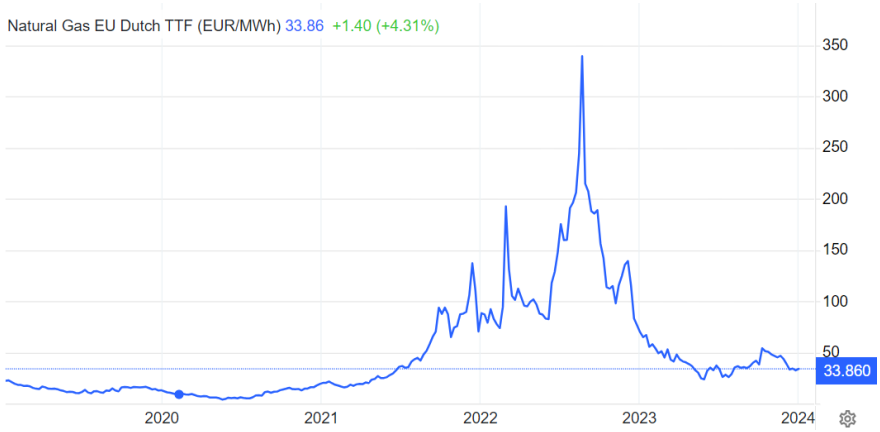

Figure 5.10: Price of natural gas in central Europe [82].

5.3 Comparative analysis with commercial technologies

This section aims to compare the SunDial with the market competitors. The solar concentrator with major capacity installed in MW and a higher number of projects is the PTC, as seen in Section 1.1. Therefore, a PTC with a similar aperture area to the SunDial 16x16 and with the same evacuated tube collector as the receiver was selected to perform a comparison. The chosen PTC is the Ultimate Trough (UT) collector [66], and the characteristics of the two collectors on the table are shown in Table 5.7.

Table 5.7: Principal data for the examine collectors

	SunDial HL	SunDial LL	Ultimate Trough
Module reflective area [m^2]	176	190	184
Module length [m]	16	16	24.5
Module width [m]	16	16	7.51
Absorber tube outer diameter[m]	0.07	0.07	0.07

The PTC is simulated with a pre-existent PTC model available in an open-source library called ThermoCycle [63]. This model has been validated in Plataforma Solar the Almería

experimental facility [26]. The ThermoCycle model, called SolAbs, is based on Forristal approach [34]. This approach is similar to the one described for the SunDial model in Section 3.1.2. The model considers the conduction and thermal energy accumulation in the absorber; the convection, and the radiation between the absorber and the glass envelope; the conduction and the thermal energy accumulation of the glass envelope; and the radiation and convection losses to the environment. The details of the PTC model are shown in Appendix E.

5.3.1 Energy comparison between the SunDial and the PTC

The model simulated considered only the solar collectors in an open circuit with a fixed inlet temperature of 190 ºC and a heat sink, so all the heat produced by collectors is counted. The mass flow through the collectors is fixed to maintain a velocity of 1 m/s, thus, the outlet temperature is variable. The PTC can be oriented in a North-South or an East-west direction. The PTC was simulated for the same low-latitude and high-latitude weather data as the SunDial 2-axes, corresponding to Corinth, Greece, and Iasi, Romania. The SunDial 1-axis was only simulated for the low latitude location due to its low efficiency in high latitudes.

According to Figure 5.11, the energy production per reflective area over a year is compared between different solar collector configurations in Greece and Romania. In Greece, the parabolic trough collector (PTC) oriented in the north-south direction exhibits the highest performance. The SunDial with two-axis tracking produces 9 % less energy than the top-performing PTC. The PTC oriented east-west produces 18.6 % less energy than the north-south PTC, while the SunDial with single-axis tracking has the lowest energy output, 33.3 % less than the north-south PTC. A similar trend is observed in Romania, where the SunDial with two-axis tracking generates 9.5 % less energy than the north-south PTC, and the east-west PTC produces 17.6 % less energy than the N/S.

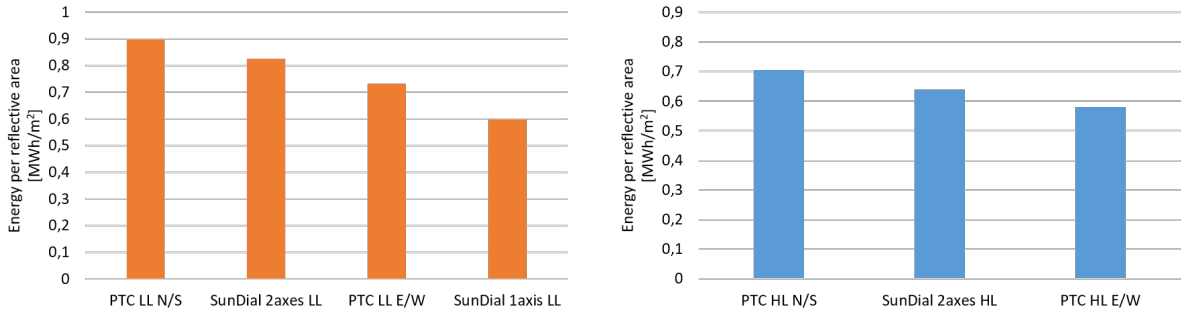

Figure 5.11: Energy per reflective area for the different solar concentrates in (a) Greece and (b) Romania.

To better understand the performance of each collector, the power results for six characteristic days from different months were plotted for the two locations. Figure 5.12 illustrates the results for the two SunDials and the PTC in both orientations for the Greek location.

During the winter days, the PTC E/W exhibits the highest peak power production, while the

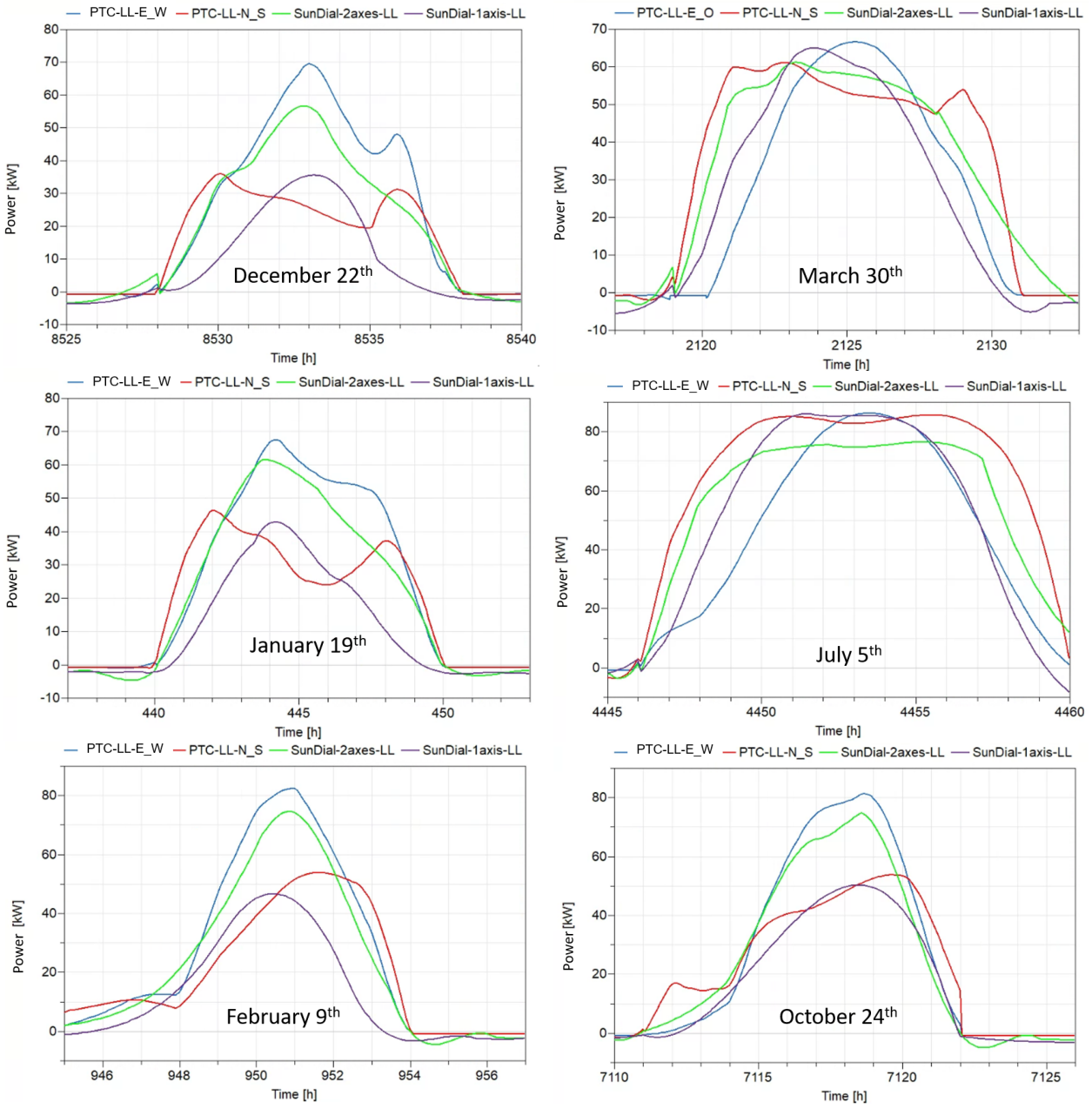

Figure 5.12: Power results in kW for six days corresponding to different months in Corinth, Greece

SunDial 2-axes presents a similar curve. The PTC N/S shows a lower maximum due to a decrease at solar noon caused by a reduction in the IAM factor. The SunDial 1-axis has fewer operation hours due to the IAM factor being zero for low sun elevations, and its maximum power is also lower.

In spring, the reduced impact of the IAM factor at midday, combined with the better performance of the N/S orientation at lower sun elevation angles, means this orientation achieves the highest energy production. The SunDial 2-axes comes in second, again demonstrating extended operating hours. Lastly, the SunDial-1 axis and the PTC E/W exhibit lower

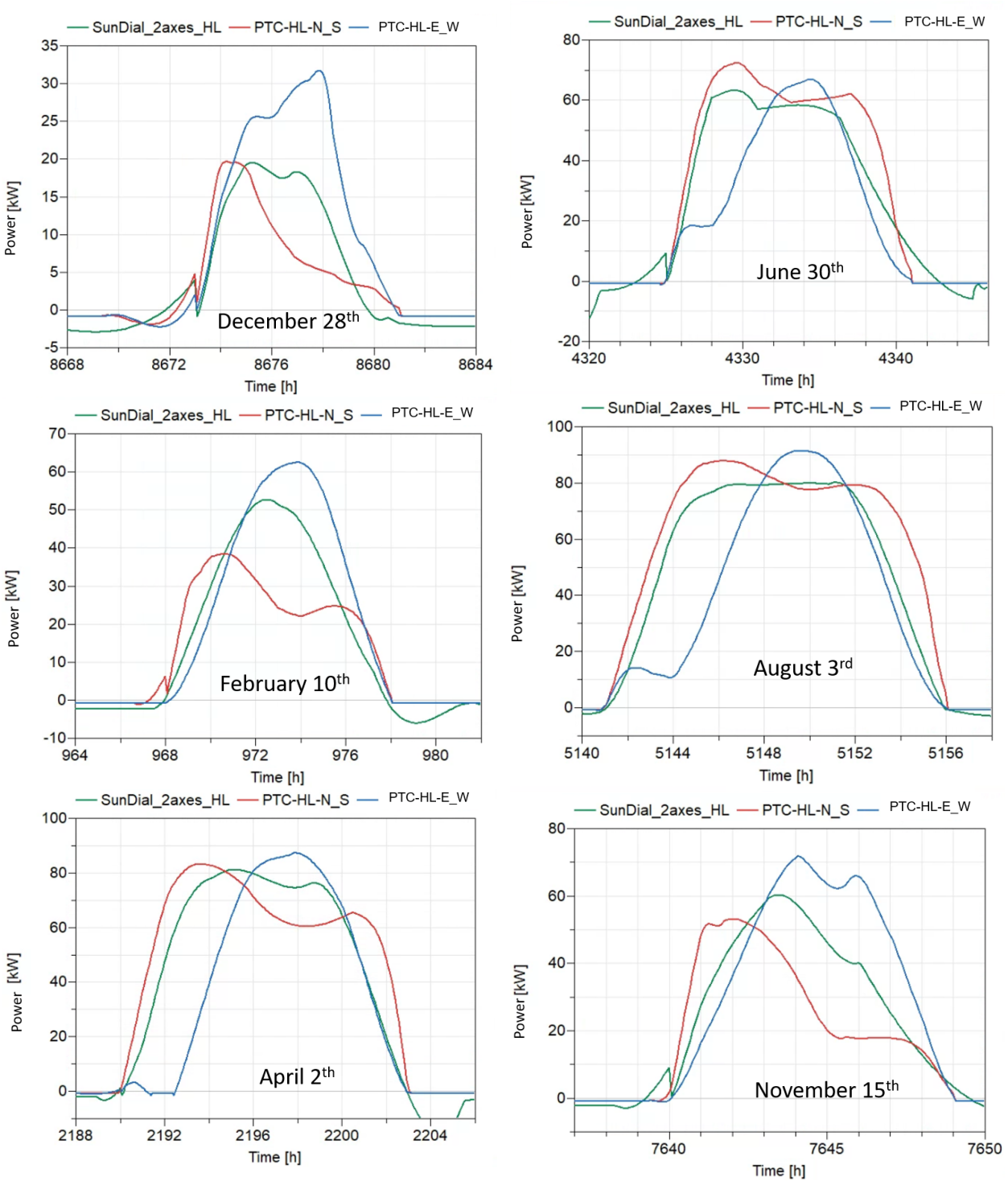

Figure 5.13: Power results in kW for six days corresponding to different months in Iasi, Romania

performance due to their reduced operating hours.

In summer, the PTC N/S stands out due to the extended hours of operation, and the maximum power achieved is similar to the PTC E/W. The SunDial 2-axes also presents an extended

operation in time, but the maximum power reached is lower due to the lower efficiency of the Fresnel collector. Finally, the PTC E/W exhibits a wider power curve than the SunDial 1-axis.

In the fall, the power curves exhibit a similar pattern to the winter scenario, with the PTC E/W and the SunDial 2-axes outperforming the PTC N/S. Summarizing, the power plots for the different seasons provide insights into the hours of operation and the maximum peak power, in addition to the amount of energy produced. The key finding is that although the SunDial 2-axes produces 9% less energy than the PTC N/S, its power curve is more consistent throughout the year. In contrast, the PTC N/S maximum power peak experiences a 50% reduction during the winter and fall seasons.

The same analysis was conducted for the location in Romania. In this scenario, the SunDial 1-axis was not considered due to its lower efficiency at low sun elevation angles. The results exhibit some similarities with the findings for the low-latitude location. For the Winter and Fall seasons, the PTC N/S demonstrates lower performance due to reduced efficiency during solar noon. The PTC E/W stands out, followed by the SunDial 2-axes. In Summer and Spring, the PTC N/S emerges as the top performer, again followed by the SunDial 2-axes. Therefore, the comparison between the collectors is independent of latitude; the PTC N/S generates more annual energy, while the SunDial 2-axes exhibits more stable energy production throughout the year.

5.3.2 LCOH comparison between the SunDial and PTC

With the results of these simulations, we can estimate the LCOH to calculate which would be the necessary price for SunDial to be a competitive alternative for PTC. This can be found by comparing the LCOH for the SunDial and the PTC calculated using different collectors' prices. Because the PTC is the most used collector, a price can be found in the literature. Then, the price of the SunDial to achieve the same LCOH can be estimated. The LCOH was calculated for a range of costs of the solar collector between 120 and 240 €/m^2, considering an operational life of 25 years, a discount rate of 5 %, maintenance and operation cost equivalent to 0.5 % of the capital cost, and a balance of plant cost of 40 €/m^2. The energy production was standardized to 1 GWh/year, allowing the determination of the required number of SunDials and PTCs to be included in the initial capital cost assessment. It was assumed that all energy generated by the collectors was utilized in the industrial process.

Figure 5.14 depicts the LCOH outcomes for the next five scenarios: the PTC with the north-south orientation in the low and high latitude locations, the SunDial with 2 tracking axes also for both locations, and finally the SunDial with one axis only for the low latitude location. The results show a lower LCOH is obtained by using solar concentrating technologies compared to natural gas. According to the literature, a reasonable price for PTC is around 200 €/m^2, which resulted in an LCOH of 19 €/MWh for the low-latitude location and 25 €/MWh for the high-latitude. To achieve comparable LCOH values, the SunDial with one axis would require a collector price of 120 €/m^2, while the SunDial with 2 axes would need a price of 180 €/m^2. Our cost estimations indicate that the SunDial 2 axes could be feasible,

but the SunDial 1 axis would necessitate enhancements in cost or efficiency.

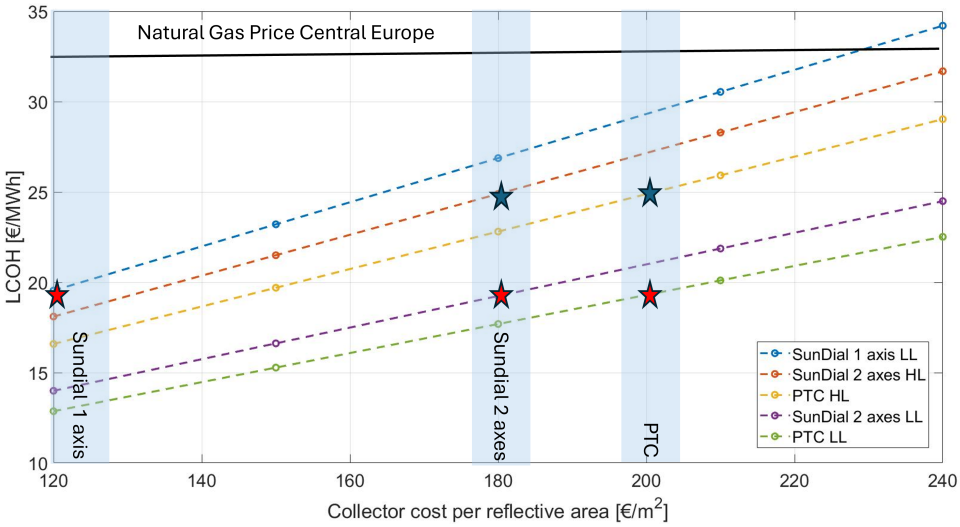

Figure 5.14: LCOH versus the cost of the solar field for PTC and the SunDial in both locations.

5.3.3 Comparison between the SunDial and the PTC applied to ASTEP

Annual simulations were conducted with the PTC orientated in the N-S direction applied to the ASTEP system to provide heat to the tube steel factory in Iasi and the dairy factory in Greece. This orientation was selected because it maximizes energy production. As it was found in the previous chapter the SunDial with two tracking axes is cheaper than the SunDial with one axis in the larger versions and, also, has a higher efficiency. This implies that is convenient to apply the SunDial with 2 axes in both locations. The results are present in terms of energy per square meter of the reflective area, facilitating a direct comparison between the PTC and SunDial, which have different areas.

For the dairy factory in Corinth, the results for the PTC and the SunDial 2-axes collectors are shown in Table 5.8. The SunDial 1-axis was also included for performance comparison, despite its lower efficiency. For the PTC, two scenarios were performed with 2 and 4 TES modules. The PTC achieves a lower LCOH with 2 TES modules, but the SunDial 2-axes presents a better performance in terms of energy produced per reflective area due to its smaller size. However, in terms of energy sent to the processes, the SunDial 2-axes show a lower value, which is attributed to the extended daily operation of the PTC. Figure 5.15 depicts the power and temperature results for the ASTEP system in the Greek dairy factory, comparing the PTC N/S and the SunDial 2-axes. The higher temperatures achieved by the PTC and its extended daily operation led to increased operating hours for the demand. Furthermore, it can be observed that the PTC requires defocusing due to the storage being full, suggesting that an increase in storage capacity, could lead to higher energy production. Figure 5.16 shows the results for the same day with 2 and 4 modules of TES, where it is noticed that

with 4 modules the PTC is always focused. However, the cost of enlarging the storage to reduce the defocus does not compensate, and a higher LCOH is obtained.

Table 5.8: Comparative table between SunDials and PTC for the dairy factory

	SunDial 1-axis	SunDial 2-axes	PTC-2TES	PTC-4TES
Reflective area [m^2]	188	176	184	184
Energy per area [kWh/m^2]	618.1	813.1	782.6	822.2
Process energy p.a. [kWh/m^2]	498.9	702.4	759.2	777.6
Cost per area [€/m^2]	190-270	190-270	150-200	150-200
LCOH [€/MWh]	32.9-44.6	23.6-31.8	18.9-23.7	21.2-25.8

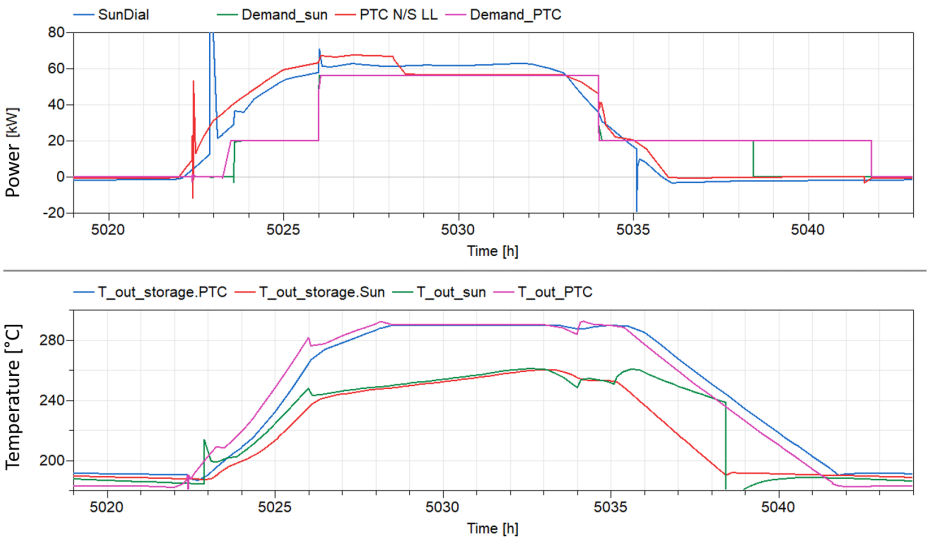

Figure 5.15: Power and Temperature results for a simulation day of the ASTEP system for the dairy factory with the PTC N/S and the SunDial 2 axes

Table 5.9 illustrates the outcomes for the tube steel factory, revealing that the total energy produced in the solar collector per unit area is nearly identical for both collectors. However, when the SunDial 2-axes is employed, the process energy is 6.3 % lower. Although the LCOH for SunDial is 3.9 €/MWh higher, it's noteworthy that both options offer a lower cost compared to natural gas.

5.4 Findings

In this chapter, a techno-economic analysis was conducted for both the SunDials and the ASTEP system. Initially, a comprehensive literature review was undertaken, revealing that the competitive price range for solar collectors typically falls between 150-200 €/m^2, aiming to rival fossil fuel alternatives. Moreover, the LCOH target was determined by benchmarking

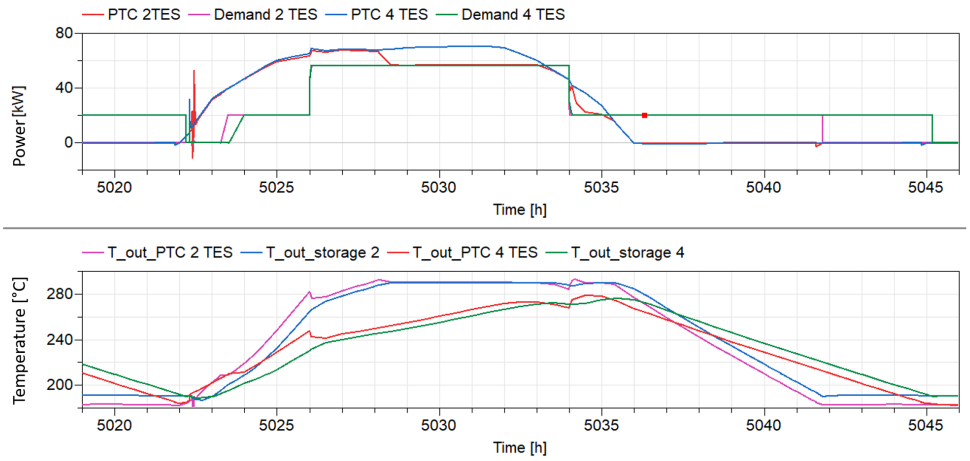

Figure 5.16: Power and Temperature results for a simulation day of the ASTEP system for the dairy factory with the PTC N/S for 2 and 4 TES modules

Table 5.9: Comparative table between SunDial 2 axes and PTC for the tube steel factory in Romania

	SunDial 2 axes HL	PTC- UT
Reflective area [m^2]	176	184
Energy per area [kWh/m^2]	642.2	644.8
Process Energy per area [kWh/m^2]	572.2	610.5
Cost per area [€/m^2]	170-250	150-200
LCOH [€/MWh]	26.4-36.54	22.4-28.4

against the fluctuating price of natural gas, which varies depending on the plant's location. For instance, in central Europe, the gas price has remained stable at 33 €/MWh over the past year.

The cost of the SunDials was estimated by considering a reduction of the prototype cost driven by economies of scale. Through this examination, it was revealed that the expenses associated with the tracking motors, rotating joints, and vent valves exert a significant influence on the overall cost of the collectors owing to their relatively small size. Consequently, two larger prototypes of the SunDial were suggested, resulting in a decrease in the price per reflective area to a lower boundary of 170 €/m^2 for the SunDial-HL 16x16 and 180 €/m^2 for the SunDial-LL 12x12. Furthermore, for the larger versions, the SunDial with 2 tracking axes (SunDial-HL) is cheaper than the SunDial with 1 tracking axis (SunDial-LL). This means that the SunDial with two axes is recommended to be applied in low latitudes over the SunDial with 1 axis.

Additionally, a sensitivity analysis was conducted on the LCOH, revealing that the most influential variables are the cost of the solar collector, solar multiple, SunDial size, and maximum temperature. The optimal configuration for achieving the lowest price entailed employing the SunDial 16x16, maintaining a maximum temperature of 290 °C, and adopting a solar multiple of 1.4. Notably, the calculated LCOH stood at a lower boundary of 26.4 €/MWh for a tube steel factory situated in Romania and 23.6 €/MWh for a dairy factory in Greece using the SunDial 2 axes in both locations. This outcome is promising as it underscores the competitiveness of this alternative in the market, given that the LCOH is below the price of natural gas.

Lastly, the SunDial 16x16 underwent a comparative analysis against a PTC by integrating a PTC model into the ASTEP dynamic model. The findings reveal that the SunDial with 2 axes demonstrates comparable performance to the PTC. However, the SunDial with 1 axis exhibits a 27 % reduction in energy production, resulting in LCOH values 14 €/MWh higher compared to the PTC. Therefore, cost optimization or efficiency improvements are necessary for SunDial with one axis to be a viable alternative to PTC technology.

Chapter 6

Conclusions and Future Works

The work of this thesis relies on increasing the reliability of solar heat for industrial process systems by designing a straightforward, easy-to-operate, and cost-effective configuration and control strategy of a system with a novel rotatory Fresnel collector and latent thermal storage. A dynamic model was developed to design the control system strategy that after will be applied to an experimental facility designed to evaluate the performance of the SunDial and replicate the operation in the factories. Finally, a techno-economic analysis was conducted which led to identifying the optimum system that minimized the LCOH and compared the SunDial with a parabolic trough collector. This chapter presents the conclusions drawn from this work including its main contributions as well as future perspectives.

6.1 Main Contributions

- An in-series configuration for the ASTEP system was designed to obtain a simple, robust, and straightforward solution to supply heat in different temperatures and power levels to a dairy factory in Greece and a steel tube factory in Rumania. This system comprises fewer components than the in-parallel configuration.
- A dynamic model was developed to design the PI controllers that were employed to regulate inlet temperature, and mass flow rate for demand, as well as defocus control for the SunDial. A detailed analysis reveals that due to its azimuthal tracking nature, the sensitivity of this controller varies according to sun elevation. In lower sun elevations the sensitivity is higher for the SunDial compared to a PTC.
- The dynamic model was used to compare the in-series versus an in-parallel configuration. The series configuration demonstrates a more resilient response to clouds compared to the parallel setup. Meanwhile, the parallel configuration exhibits quicker start-ups without experiencing TES inertia. Regarding the ASTEP system, preference was given to the series configuration due to its requirement for fewer components and simplified control. Conversely, in the parallel configuration, selecting TES state of charge involves three-way valves and an additional pump is needed to control the mass flow through

the TES. In contrast in the series configuration, the state of charge of the system is auto-regulated by the balance of temperatures in the system, so the number of modes of operation is reduced. Switching focus onto energy production comparisons between both configurations reveals that the parallel configuration yields 1.6% more energy for the dairy factory and 4% more for tube steel. However, there is also a higher energy consumption by the pumping system, resulting in an equal overall output of energy from both configurations when this extra usage is subtracted.

- The dynamic model was employed to examine the impact of piping thermal inertia within the system. Findings indicate that this inertia is substantial and influenced by irradiation levels; neglecting the thermal inertia of the piping might lead to an overestimation of energy production by 18% in winter. The collector and piping thermal inertia cause delays during start-up, as they require additional energy for preheating, particularly in scenarios with low irradiation
- A simplified model was obtained which reduced the simulation time for 3 days from 8 hours to just 1 minute. The modifications involved reducing the calculation nodes for SunDial, utilizing average properties for the HTF, and consolidating equations related to TES. When comparing results obtained from both models across different seasons, it was observed that energy production by SunDial and demand were identical in summer, with a 1% difference present in fall and 2% in winter. However, when analyzing the control strategy, varied results were obtained for fall and winter scenarios with delays of up to 18 minutes during process start-up. This underscores the significance of using dynamic simulation for assessing control systems while simplified annual models can provide an overall understanding of the system.
- The results from the annual simulation indicate that the system experienced substantial thermal losses, accounting for 35-40 % of the total energy generated. These losses are primarily attributed to the small scale of the SunDial. Increasing its size and power relative to the plant's piping would result in a reduced percentage of thermal losses. Regarding the control strategy, the effectiveness of flexible heating with dual supply levels was demonstrated by generating 7 % more energy compared to using only one supply level. The single level is simulated by employing only one heat exchanger operating at the higher power and temperature level.
- The experimental installation was designed to calculate seven different KPIs to evaluate the performance of the SunDials and test the control strategy designed for the end-users by three different sequential experiments. The maximum uncertainty for the experiments is in the SunDial efficiency and power calculation of 3 % and 1.1 % respectively.
- An estimation was made on the cost of the SunDials, revealing a high cost per reflective area that would pose challenges in terms of market competitiveness. This is primarily attributed to the small scale of the SunDial, leading to a lack of amortization per area for costly components such as motors and rotating joints. Scaling up the size of the SunDial would result in the distribution of these component costs over a larger area, thereby reducing the cost per reflective area. The optimal size for SunDial- with one tracking axis is determined to be 12x12 platform with associated costs ranging

from 184.5 to 270€/m^2. As for SunDial with 2 tracking axes), optimal dimensions are achieved at 16x16 with costs spanning between 169.5 and 265 €/m^2. In comparison to SunDia- 1axis, SunDia- 2 axes presents lower costs due to its lighter structure which allows better amortization of higher motor numbers. While the SunDial- 1axis tilting at 10 º entails a larger structure. This implies that is convenient to apply the SunDial with two tracking axes also in low latitudes.

- The critical variables to reduce the LCOH of the ASTEP system are the size of SunDial, solar multiple, and maximum defocus temperature. For the SunDial with 2 tracking axes, for the 16x16 size with a solar multiple of 1.4 and a maximum temperature of 290 °C, the LCOH ranged between 26.4-36.54 for the tube steel factory and 23.6-31.8 €/MWh for dairy factory—lower than the current natural gas price of 33 €/MWh. In contrast, for the SunDial with 1 tracking axis, the LCOH was between 33 and 44.6 €/MWh which is comparable to natural gas prices only in the lower boundary price estimation.
- The comparison between SunDial and the parabolic trough collector shows that the SunDial with two tracking axes can attain comparable LCOH prices for 180 €/m^2, falling within the estimated price range. On the other hand, the SunDial with one tracking axis will need to be priced at 120 €/m^2, which is below the estimated range

6.2 Future Work

The outcomes of the SunDial collector testing will determine if the expected performance and medium temperatures are attained. Additionally, the control strategy can be applied, and an evaluation of the SunDial's integration with an industrial process can be conducted. The test results will serve to validate the dynamic model of the SunDial as well as the ASTEP system model.

Once the model has been validated, it will be important to explore the potential use of SunDial with two tracking axes at higher latitude locations and compare the outcomes with the cost of natural gas and other renewable energy alternatives. Additionally, assessing the feasibility of utilizing alternative heat transfer fluids such as water with glycol or silicon instead of thermal oil is essential. Thermal oils come with certain drawbacks including being a pollutant and a flammable chemical substance. The choice to use thermal oil was influenced by the sub-zero temperatures experienced during winter in Romania which make using water unfeasible. Furthermore, exploring its integration with other industrial processes requiring medium temperatures different from those studied here could also be considered.

The SunDial implies challenges in terms of both expense and effectiveness because of its compact size. Exploring the potential construction of a larger version, such as the SunDial with two axes, could be beneficial. Scaling up the device would lower the cost per reflective area and decrease thermal losses, ultimately enhancing overall efficiency. Additional immediate enhancements for the SunDial with two axes could involve cost reduction measures like utilizing a single motor for mirror tracking instead of using one motor per mirror.

The SunDial with one tracking axis falls short of meeting the target for LCOH competitiveness compared to other market solutions. Consequently, further efforts are required to enhance efficiency or minimize the cost per reflective area. One potential approach is to assess whether reducing the tilt of the collector in larger versions could help decrease the LCOH.

References

Bibliography

[1] R. Abbas, M. J. Montes, A. Rovira, and J. M. Martínez-Val, "Parabolic trough collector or linear Fresnel collector? A comparison of optical features including thermal quality based on commercial solutions," *Solar Energy*, vol. 124, pp. 198–215, Feb. 2016. DOI: 10.1016/J.SOLENER.2015.11.039.

[2] R. Abbas, "D5.2 System component and final integration design report," Tech. Rep. 884411, 2022.

[3] R. Abbas, R. Barbero, A. Rovira, and M. Barnetche, "SunDial, a new collector for solar heat for industrial processes: Optical and thermal design," 2023. DOI: 10.1016/j.tsep.2023.102025. [Online]. Available: https://doi.org/10.1016/j.tsep.2023.102025.

[4] R. Abbas, M. J. Montes, and J. Cano, "Enhancement of SunDial optical performance handling cosine and end losses," vol. 2445, p. 140 001, 2022. DOI: 10.1063/5.0085667. [Online]. Available: https://doi.org/10.1063/5.0085667.

[5] R. Abbas, M. J. Montes, J. C. Nogueras, *et al.*, "Enhancement of SunDial optical performance handling cosine and end losses," SolarPaces, 2020.

[6] R. Abbas, A. Rovira, M. Ibarra, *et al.*, "D3.3 Design of the daily and yearly operation for AMTP and MAND & D5.1 Report on the integrated ASTEP model development and Conceptual Designs," Tech. Rep. 884411, 2021, pp. 1–112.

[7] J. C. Arroyo, "DISEÑO DE DETALLE DE UN CONCENTRADOR SOLAR SUNDIAL PARA PROCESOS," Ph.D. dissertation, Universidad Politécnica de Madrid, 2023.

[8] *ASTEP*. [Online]. Available: https://astepproject.eu/.

[9] K. J. Åström and T. Hägglund, *PID controllers: theory, design, and tuning*, 1995.

[10] R. Barbero, A. Rovira, M. J. Montes, and J. M. Martínez Val, "A new approach for the prediction of thermal efficiency in solar receivers," *Energy Conversion and Management*, vol. 123, pp. 498–511, 2016. DOI: 10.1016/j.enconman.2016.06.065.

[11] M. Barnetche, L. F. González-Portillo, and R. Abbas, "Optimum integration of latent heat storage in a solar thermal system for industrial processes: In series or in parallel?," 2023. DOI: 10.1016/j.applthermaleng.2023.121090. [Online]. Available: https://doi.org/10.1016/j.applthermaleng.2023.121090.

[12] M. Barnetche, L. F. González-Portillo, J. Muñoz-Antón, *et al.*, "Analysis of the thermal inertia of pipelines in SHIP," *Results in Engineering*, p. 100 908, Jan. 2023. DOI: 10.1016/J.RINENG.2023.100908. [Online]. Available: https://linkinghub.elsevier.com/retrieve/pii/S259012302300035X.

[13] E. Bellos and C. Tzivanidis, "Assessment of linear solar concentrating technologies for Greek climate," 2018. DOI: 10.1016/j.enconman.2018.06.076. [Online]. Available: https://doi.org/10.1016/j.enconman.2018.06.076.

[14] M. Biencinto, R. Bayón, L. González, R. Christodoulaki, and E. Rojas, "Integration of a parabolic-trough solar field with solid-solid latent storage in an industrial process with different temperature levels," *Applied Thermal Engineering*, vol. 184, p. 116 263, Feb. 2021. DOI: 10.1016/J.APPLTHERMALENG.2020.116263.

[15] M. Biencinto, L. González, and L. Valenzuela, "Simulation and Economic Analysis of an Innovative Compact Linear Fresnel Collector Coupled to Two Industrial Processes with Low and Medium Temperatures," *27th SolarPACES Conference, September 27 – October 1, 2021, Online Event*, 2021.

[16] M. Bolognese, D. Viesi, R. Bartali, and L. Crema, "Modeling study for low-carbon industrial processes integrating solar thermal technologies. A case study in the Italian Alps: The Felicetti Pasta Factory," *Solar Energy*, vol. 208, pp. 548–558, Sep. 2020. DOI: 10.1016/J.SOLENER.2020.07.091.

[17] E. F. Camacho, F. R. Rubio, M. Berenguel, and L. Valenzuela, "A survey on control schemes for distributed solar collector fields. Part I: Modeling and basic control approaches," *Solar Energy*, vol. 81, no. 10, pp. 1240–1251, 2007. DOI: 10.1016/j.solener.2007.01.002.

[18] J. Cano-nogueras, J. Muñoz-antón, and J. M. Martinez-val, "A new thermal-solar field configuration: The rotatory fresnel collector or sundial," *Energies*, vol. 14, no. 14, 2021. DOI: 10.3390/en14144139.

[19] F. Casella and P. Milano, "The ThermoPower Library," [Online]. Available: https://build.openmodelica.org/Documentation/ThermoPower.html.

[20] *Convenio colectivo de la construcción en Madrid*. [Online]. Available: https://www.bocm.es/boletin/CM_Orden_BOCM/2021/04/29/BOCM-20210429-31.PDF.

[21] A. Crespo, C. Barreneche, M. Ibarra, and W. Platzer, "Latent thermal energy storage for solar process heat applications at medium-high temperatures – A review," *Solar Energy*, vol. 192, pp. 3–34, Nov. 2019. DOI: 10.1016/J.SOLENER.2018.06.101.

[22] A. Crespo, I. Muñoz, W. Platzer, and M. Ibarra, "Integration enhancements of a solar parabolic trough system in a Chilean juice industry: Methodology and case study," *Solar Energy*, vol. 224, pp. 593–606, Aug. 2021. DOI: 10.1016/J.SOLENER.2021.03.041.

[23] I. Cruz-Robles, J. M. Islas-Samperio, E. Alonso, A. J. Vázquez-Vaamonde, C. A. Pérez-Rábago, and C. A. Estrada, "Reducing CO2 emissions in the copper smelting process by using high-temperature solar heat: Tecno-economic assessment," *Applied Thermal Engineering*, vol. 226, May 2023. DOI: 10.1016/J.APPLTHERMALENG.2023.120270.

[24] E. Dahlquist, E. T. Aparicio, H. Li, P. Fritzson, and P. Östlund, "Comparison Open Modelica – Dymola for Power Plant Simulation," *SNE Simulation Notes Europe*, vol. 23, no. 3-4, pp. 139–146, 2015. DOI: 10.11128/sne.23.tn.10207.

[25] Dassult Systems, *Dymola*. [Online]. Available: https://www.3ds.com/products/catia/dymola.

[26] A. Desideri, R. Dickes, J. Bonilla, L. Valenzuela, S. Quoilin, and V. Lemort, "Steady-state and dynamic validation of a parabolic trough collector model using the ThermoCycle Modelica library," *Solar Energy*, vol. 174, pp. 866–877, Nov. 2018. DOI: 10.1016/J.SOLENER.2018.08.026.

[27] Eastman Chemical Company, *Therminol 59*, 2021.
[28] J. Eddouibi, S. Abderafi, S. Vaudreuil, and T. Bounahmidi, "Dynamic simulation of solar-powered ORC using open-source tools: A case study combining SAM and coolprop via Python," *Energy*, vol. 239, p. 121 935, Jan. 2022. DOI: 10.1016/J.ENERGY.2021.121935.
[29] EDF, *ThermoSysPro*.
[30] B. El Ghazzani, D. Martinez Plaza, R. Ait El Cadi, A. Ihlal, B. Abnay, and K. Bouabid, "Thermal plant based on parabolic trough collectors for industrial process heat generation in Morocco," *Renewable Energy*, vol. 113, pp. 1261–1275, 2017. DOI: 10.1016/j.renene.2017.06.063. [Online]. Available: http://dx.doi.org/10.1016/j.renene.2017.06.063.
[31] Electric Power Research Institute, "Program on Technology Innovation : Evaluation of," Tech. Rep., 2009.
[32] B. Epp, M. Oropeza, and M. Taylor, "Cost trends of solar energy for heat in industry," 2021. [Online]. Available: https://www.solar-payback.com/.
[33] G. Espinosa-Rueda, J. Luis, N. Hermoso, N. Martínez-Sanz, and M. Gallas-Torreira, "Vacuum evaluation of parabolic trough receiver tubes in a 50 MW concentrated solar power plant," 2016. DOI: 10.1016/j.solener.2016.09.017. [Online]. Available: http://dx.doi.org/10.1016/j.solener.2016.09.017.
[34] R. Forristall, "Heat Transfer Analysis and Modeling of a Parabolic Trough Solar Receiver Implemented in Engineering Equation Solver," no. October, p. 164, 2003. DOI: NREL/TP-550-34169.
[35] R. Franke, F. Casella, M. Otter, *et al.*, "Stream Connectors – An Extension of Modelica for Device-Oriented Modeling of Convective Transport Phenomena," *Proceedings of the 7 International Modelica Conference Como, Italy*, vol. 43, pp. 108–121, 2009. DOI: 10.3384/ecp09430078.
[36] R. Gabbrielli, P. Castrataro, F. Del Medico, M. Di Palo, and B. Lenzo, "Levelized cost of heat for linear Fresnel concentrated solar systems," *Energy Procedia*, vol. 49, pp. 1340–1349, 2014. DOI: 10.1016/j.egypro.2014.03.143. [Online]. Available: http://dx.doi.org/10.1016/j.egypro.2014.03.143.
[37] J. D. Gil, A. Topa, J. D. Álvarez, J. L. Torres, and M. Pérez, "A review from design to control of solar systems for supplying heat in industrial process applications," *Renewable and Sustainable Energy Reviews*, vol. 163, no. April, p. 112 461, 2022. DOI: 10.1016/j.rser.2022.112461. [Online]. Available: https://doi.org/10.1016/j.rser.2022.112461.
[38] F. Giovannetti, P. Horta, H. Marthy, *et al.*, "Comparison of process heat collectors with respect to technical and economic conditions," *IEA SHC Task 49 - Solar Process Heat for Production and Advanced Applications*, 2016.
[39] M. V. Guisado, F. Zaversky, I. Santana, and A. Bernardos, "SOLAR HEAT FOR INDUSTRIAL PROCESSES (SHIP): MODELING AND OPTIMIZATION OF A PARABOLIC TROUGH PLANT WITH THERMOCLINE THERMAL STORAGE SYSTEM TO SUPPLY MEDIUM TEMPERATURE PROCESS HEAT," 2016. DOI: 10.18086/eurosun.2016.02.22. [Online]. Available: http://proceedings.ises.org.
[40] Hilding Elmqvist, "Modelica — A unified object-oriented language for physical systems modeling," Tech. Rep. 6, 1997, p32. DOI: 10.1016/s0928-4869(97)84257-7.
[41] T. Hirsch, J. Dersch, T. Fluri, *et al.*, "SolarPACES guideline for bankable STE yield assessment," *IEA-SolarPACES*, p. 190, 2017.

[42] IEA, "Key World Energy Statistics 2021 – Statistics Report," *IEA Publications*, pp. 1–82, 2021.

[43] IEA, "Net Zero by 2050: A Roadmap for the Global Energy Sector," *International Energy Agency*, p. 224, 2021. [Online]. Available: https://www.iea.org/reports/net-zero-by-2050.

[44] IEA Task 49/IV, *SHIP plats database*. [Online]. Available: http://ship-plants.info/?collector_type=5&industry_sector=4.

[45] IEA-ETSAP, "Thermal Energy Storage-Insights for Policy Makers," *IEA ETSAP - Technology Brief*, no. January, p. 9, 2013.

[46] J. Immonen and K. M. Powell, "Dynamic optimization with flexible heat integration of a solar parabolic trough collector plant with thermal energy storage used for industrial process heat," *Energy Conversion and Management*, vol. 267, p. 115 921, 2022. DOI: 10.1016/j.enconman.2022.115921. [Online]. Available: https://doi.org/10.1016/j.enconman.2022.115921.

[47] IRNEA, *Renewable Power Generation Costs in 2021*. 2022, p. 160. [Online]. Available: https://www.irena.org/-/media/Files/IRENA/Agency/Publication/2018/Jan/IRENA_2017_Power_Costs_2018.pdf.

[48] M. Kavouras and M. Kokla, "Integration Guidelines," *Theories of Geographic Concepts*, no. February, pp. 253–292, 2007. DOI: 10.1201/9781420004670.ch16.

[49] B. Koçak, A. I. Fernandez, and H. Paksoy, "Review on sensible thermal energy storage for industrial solar applications and sustainability aspects," *Solar Energy*, vol. 209, pp. 135–169, Oct. 2020. DOI: 10.1016/J.SOLENER.2020.08.081.

[50] P. Ktistis, R. A. Agathokleous, and S. A. Kalogirou, "A design tool for a parabolic trough collector system for industrial process heat based on dynamic simulation," *Renewable Energy*, vol. 183, pp. 502–514, Jan. 2022. DOI: 10.1016/j.renene.2021.11.040.

[51] L. Kumar, J. Ahmed, M. El Haj Assad, and M. Hasanuzzaman, "Prospects and Challenges of Solar Thermal for Process Heating: A Comprehensive Review," *Energies*, vol. 15, no. 22, Nov. 2022. DOI: 10.3390/EN15228501.

[52] P. Kurup, S. Glynn, and S. Akar, "Manufacturing cost analysis of advanced parabolic trough collector," *AIP Conference Proceedings*, vol. 2445, no. May, 2022. DOI: 10.1063/5.0085663.

[53] P. Kurup and C. Turchi, "Case study of a californian brewery to potentially use concentrating solar power for renewable heat generation," *Proceedings of the ISES Solar World Congress 2019 and IEA SHC International Conference on Solar Heating and Cooling for Buildings and Industry 2019*, pp. 560–571, 2020. DOI: 10.18086/swc.2019.12.07.

[54] P. Kurup and C. S. Turchi, "Parabolic Trough Collector Cost Update for the System Advisor Model (SAM)," *Technical Report NREL/TP-6A20-65228 National Renewable Energy Laboratory*, no. November, pp. 1–40, 2015. [Online]. Available: http://www.nrel.gov/docs/fy16osti/65228.pdf.

[55] B. Lamrani and A. Draoui, "Modelling and simulation of a hybrid solar-electrical dryer of wood integrated with latent heat thermal energy storage system," *Thermal Science and Engineering Progress*, vol. 18, p. 100 545, Aug. 2020. DOI: 10.1016/J.TSEP.2020.100545.

[56] Lawrence Berkeley National Laboratory, *Modelica Buildings Library*, 1998. [Online]. Available: https://simulationresearch.lbl.gov/modelica/.

[57] McKinsey & Company, "Net-Zero Europe," pp. 1–204, 2020.

[58] NREL, *System Advisor Model*, 2018. [Online]. Available: https://sam.nrel.gov.

[59] M. C. Oliveira and M. Iten, "Modelling of A Solar Thermal Energy System For Energy Efficiency Improvement In A Ceramic Plant," DOI: 10.1051/rees/2021029. [Online]. Available: https://doi.org/10.1051/rees/2021029.

[60] F. Ordóñez, E. Flores, and R. Soria, "Comprehensive analysis of the variables influencing the techno-economic optimization of medium temperature linear Fresnel collectors," *Energy Reports*, vol. 7, pp. 5747–5761, Nov. 2021. DOI: 10.1016/J.EGYR.2021.08.194.

[61] R. Pitz-Paal, J. Krüger, J. Hinsch, *et al.*, "Decarbonizing the German industrial thermal energy use with solar, hydrogen, and other options–Recommendations for the world," *Solar Compass*, vol. 3-4, p. 100 029, Sep. 2022. DOI: 10.1016/J.SOLCOM.2022.100029.

[62] D. Pulido-Iparraguirre, L. Valenzuela, J. J. Serrano-Aguilera, and A. Fernández-García, "Optimized design of a Linear Fresnel reflector for solar process heat applications," *Renewable Energy*, vol. 131, pp. 1089–1106, 2019. DOI: 10.1016/j.renene.2018.08.018.

[63] S. Quoilin, A. Desideri, J. Wronski, I. Bell, and V. Lemort, "ThermoCycle: A Modelica library for the simulation of thermodynamic systems," *Proceedings of the 10th International Modelica Conference, March 10-12, 2014, Lund, Sweden*, vol. 96, pp. 683–692, 2014. DOI: 10.3384/ecp14096683.

[64] R. Ramirez Javier, J. M. Cardemil, I. Calderón-Vásquez, *et al.*, "Assessing the Uncertainties of Simulation Approaches for Solar Thermal Systems Coupled to Industrial Processes," 2022. DOI: 10.3390/en15093333. [Online]. Available: https://doi.org/10.3390/en15093333.

[65] K. Ravi Kumar, N. V. Krishna Chaitanya, and N. Sendhil Kumar, "Solar thermal energy technologies and its applications for process heating and power generation – A review," *Journal of Cleaner Production*, vol. 282, p. 125 296, Feb. 2021. DOI: 10.1016/J.JCLEPRO.2020.125296.

[66] K. Riffelmann, T. Richert, P. Nava, and A. Schweitzer, "Ultimate Trough® - A significant step towards cost-competitive CSP," *Energy Procedia*, vol. 49, pp. 1831–1839, 2014. DOI: 10.1016/j.egypro.2014.03.194.

[67] S. Rodat, J. V. Souza, S. Thebault, V. Vuillerme, and N. Dupassieux, "Dynamic simulations of Fresnel solar power plants," *Energy Procedia*, vol. 49, pp. 1501–1510, 2014. DOI: 10.1016/j.egypro.2014.03.159. [Online]. Available: http://dx.doi.org/10.1016/j.egypro.2014.03.159.

[68] A. Rovira, R. Abbas, R. Barbero, *et al.*, "D3.1 Preliminary design of Sundial for AMTP," Tech. Rep. 884411, 2021, pp. 1–23.

[69] A. Rovira, R. Abbas, R. Barbero, *et al.*, "D3.2 Preliminary design of Sundial for MAN," no. 884411, pp. 1–23, 2021.

[70] H. H. Sait, J. M. Martinez-Val, R. Abbas, and J. Munoz-Anton, "Fresnel-based modular solar fields for performance/cost optimization in solar thermal power plants: A comparison with parabolic trough collectors," *Applied Energy*, vol. 141, pp. 175–189, 2015. DOI: 10.1016/j.apenergy.2014.11.074. [Online]. Available: http://dx.doi.org/10.1016/j.apenergy.2014.11.074.

[71] A. J. Sánchez, A. J. Gallego, J. M. Escaño, and E. F. Camacho, "Event-based MPC for defocusing and power production of a parabolic trough plant under power limitation," *Solar Energy*, vol. 174, no. August, pp. 570–581, 2018. DOI: 10.1016/j.solener.2018.09.044. [Online]. Available: https://doi.org/10.1016/j.solener.2018.09.044.

[72] A. Sandá, S. L. Moya, and L. Valenzuela, "Modelling and simulation tools for direct steam generation in parabolic-trough solar collectors: A review," *Renewable and Sustainable Energy Reviews*, vol. 113, p. 109 226, Oct. 2019. DOI: 10.1016/J.RSER.2019.06.033.

[73] K. Sartor and R. Dickes, "Experimental validation of heat transport modelling in large solar thermal plants," *Energies*, vol. 13, no. 9, 2020. DOI: 10.3390/en13092343.

[74] M. H. Sidek, W. Z. Hasan, M. Z. Kadir, *et al.*, "GPS based portable dual-axis solar tracking system using astronomical equation," *Conference Proceeding - 2014 IEEE International Conference on Power and Energy, PECon 2014*, pp. 245–249, 2014. DOI: 10.1109/PECON.2014.7062450.

[75] R. Silva, M. Pérez, and A. Fernández-Garcia, "Modeling and co-simulation of a parabolic trough solar plant for industrial process heat," *Applied Energy*, vol. 106, pp. 287–300, 2013. DOI: 10.1016/j.apenergy.2013.01.069. [Online]. Available: http://dx.doi.org/10.1016/j.apenergy.2013.01.069.

[76] J. P. Solano-Fernández, J. Muñoz-Camara, H. Hammou, A. Dmitruk, and P. Kew, "D4.1 Engineering configuration of the thermal energy storage system," Tech. Rep. 884411, 2020, pp. 1–33.

[77] *Solar Payback Project*. [Online]. Available: https://www.solar-payback.com/potencial/?lang=es.

[78] W. Spork-Dur, "Solar Heat World Wide," p. 88, 2022. [Online]. Available: https://www.iea-shc.org/Data/Sites/1/publications/Solar-Heat-Worldwide-2021.pdf.

[79] J. Sun, Z. Zhang, L. Wang, Z. Zhang, and J. Wei, "Comprehensive Review of Line-Focus Concentrating Solar Thermal Technologies: Parabolic Trough Collector (PTC) vs Linear Fresnel Reflector (LFR)," *Journal of Thermal Science*, vol. 29, no. 5, pp. 1097–1124, Oct. 2020. DOI: 10.1007/S11630-020-1365-4/METRICS. [Online]. Available: https://link.springer.com/article/10.1007/s11630-020-1365-4.

[80] N. S. Suresh and B. S. Rao, "Solar energy for process heatingA case study of select Indian industries," *Journal of Cleaner Production*, vol. 151, no. May 2011, pp. 439–451, 2017. DOI: 10.1016/j.jclepro.2017.02.190. [Online]. Available: http://dx.doi.org/10.1016/j.jclepro.2017.02.190.

[81] R. Tascioni, M. Pirro, A. Arteconi, *et al.*, "Prediction of the time constant of small-scale concentrated solar CHP plants," *E3S Web of Conferences*, vol. 238, 2021. DOI: 10.1051/e3sconf/202123801001.

[82] *Traiding Economics*. [Online]. Available: https://tradingeconomics.com/commodity/eu-natural-gas.

[83] A. Urquía and C. Martín, "Modeling and Simulation in Engineering," *Modeling and Simulation in Engineering*, 2012. DOI: 10.5772/1415.

[84] M. Wetter and C. Haugstetter, "MODELICA VERSUS TRNSYS-A COMPARISON BETWEEN AN EQUATION-BASED AND A PROCEDURAL MODELING LANGUAGE FOR BUILDING ENERGY SIMULATION,"

[85] İ. H. Yılmaz, M. S. Söylemez, and R. Yumrutaş, "Experimental analysis and dynamic simulation of a solar-assisted industrial process using parabolic trough solar collectors under outdoor conditions," *Energy for Sustainable Development*, vol. 72, no. September 2022, pp. 212–229, 2023. DOI: 10.1016/j.esd.2022.12.017.

[86] G. Zhu, T. Wendelin, M. J. Wagner, and C. Kutscher, "History, current state, and future of linear Fresnel concentrating solar collectors," *Solar Energy*, vol. 103, pp. 639–652,

2014. DOI: 10.1016/j.solener.2013.05.021. [Online]. Available: http://dx.doi.org/10.1016/j.solener.2013.05.021.

Annexes

A - Thermal oil properties

In this appendix, the equations are used to model the thermal oil properties. These equations were obtained by approximation from the data of the company.

Therminol 55

$$\rho = -0.7261 \cdot T + 892.27 \tag{A.1}$$
$$c_p = 3.52 \cdot T + 1838.7 \tag{A.2}$$
$$k = -0.000117 \cdot T + 0.131 \tag{A.3}$$
$$\mu = \left(-161984886419\frac{1}{T^4} + 2077594474\frac{1}{T^3} - 8728754\frac{1}{T^2} + 17293\frac{1}{T} - 21\right) \tag{A.4}$$

Therminol 59

$$\rho = -0.7996 \cdot T + 997.87 \tag{A.5}$$
$$c_p = 3.383 \cdot T + 1599.1 \tag{A.6}$$
$$k = -0.000119 \cdot T + \quad 0.128 \tag{A.7}$$
$$\mu = \left(88876622821.00\frac{1}{T^4} - 704484015.60\frac{1}{T^3} + 2108897.96\frac{1}{T^2} - 1081.20\frac{1}{T} \ - 9.91\right) \tag{A.8}$$

B - Piping and Instruments Diagram

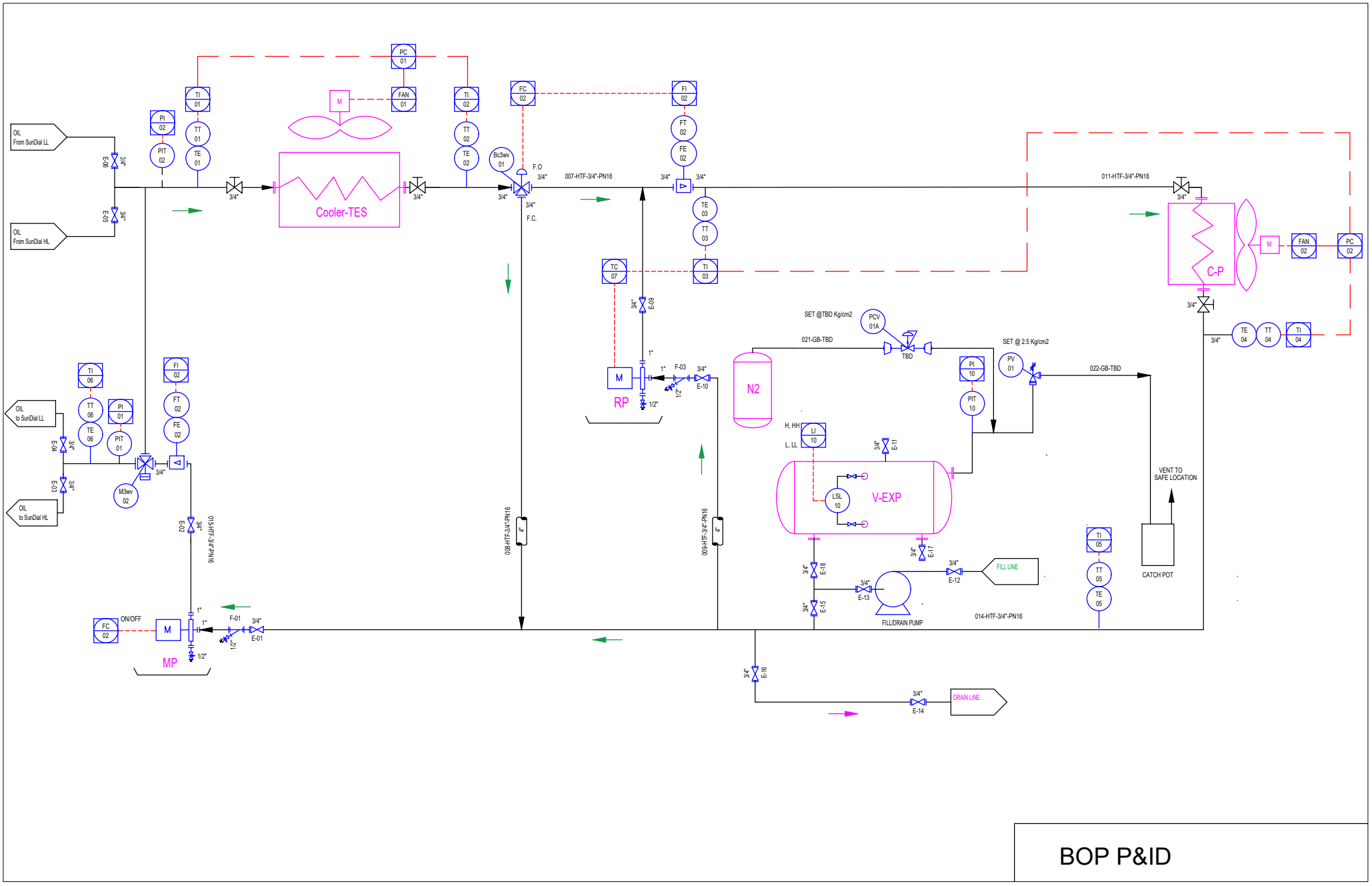
OIL
From SunDial LL
OIL
From SunDial HL
E-06
E-05
3/4"
PI
02
PIT
02
TI
01
TT
01
TE
01
PC
01
FAN
01
M
Cooler-TES
TI
02
TT
02
TE
02
FC
02
Bc3wv
01
F.O
F.C.
007-HTF-3/4"-PN16
FI
02
FT
02
FE
02
TE
03
TT
03
TI
03
TC
07
E-09
011-HTF-3/4"-PN16
C-P
FAN
02
PC
02
TE
04
TT
04
TI
04
SET @TBD Kg/cm2
PCV
01A
TBD
021-GB-TBD
SET @ 2.5 Kg/cm2
PV
01
022-GB-TBD
PI
10
PIT
10
N2
RP
F-03
E-10
1"
1/2"
3/4"
H, HH
L, LL
LI
10
LSL
10
V-EXP
E-11
E-17
E-18
E-15
E-12
E-13
FILL LINE
FILL/DRAIN PUMP
014-HTF-3/4"-PN16
VENT TO
SAFE LOCATION
CATCH POT
TI
05
TT
05
TE
05
E-16
E-14
DRAIN LINE
OIL
to SunDial LL
OIL
to SunDial HL
E-04
E-03
TI
06
TT
06
TE
06
PI
01
PIT
01
FI
02
FT
02
FE
02
M3wv
02
E-02
015-HTF-3/4"-PN16
008-HTF-3/4"-PN16
009-HTF-3/4"-PN16
4"
FC
02
ON/OFF
M
MP
F-01
E-01

BOP P&ID

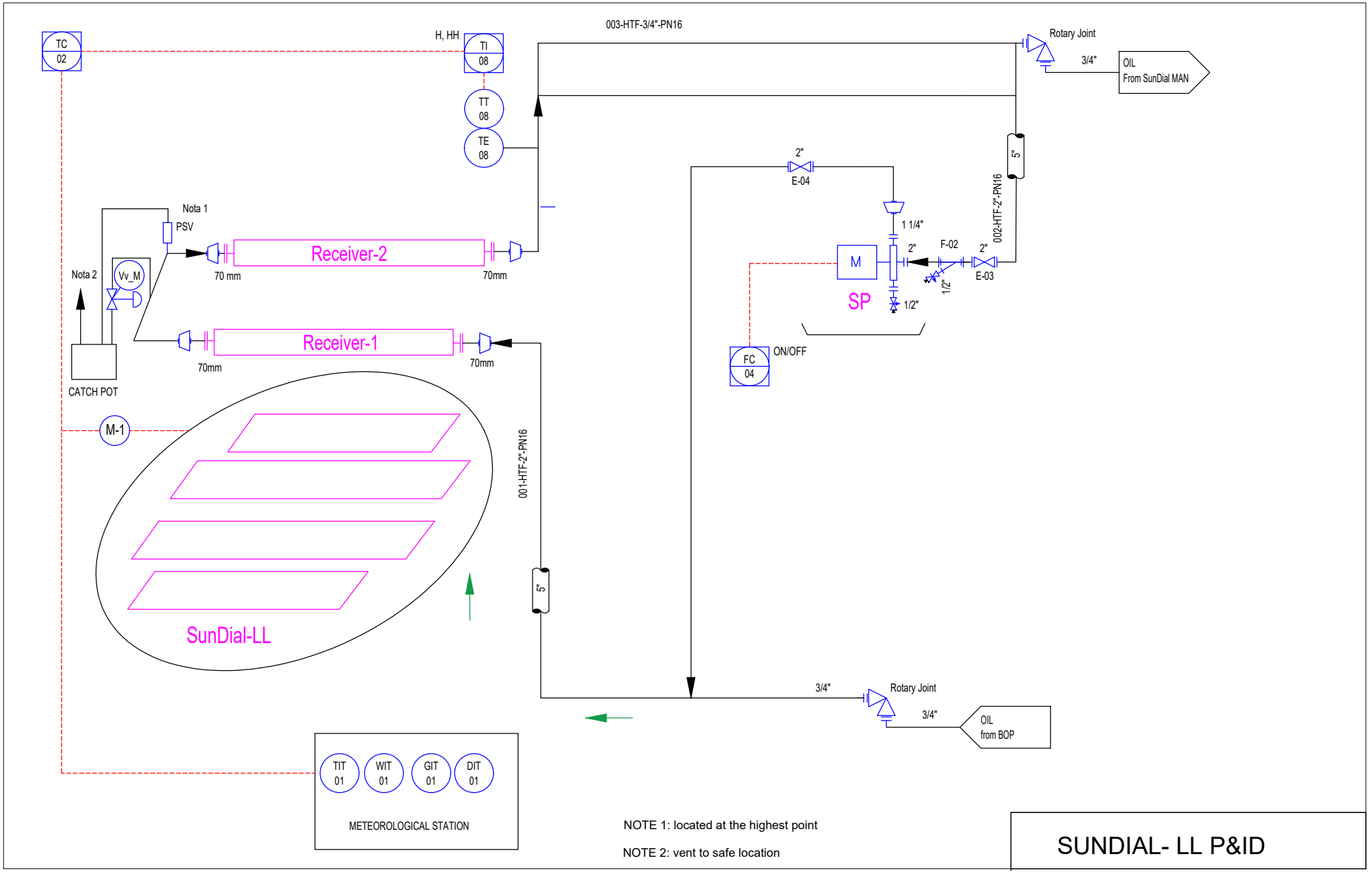
TC
02
H, HH
TI
08
TT
08
TE
08
003-HTF-3/4"-PN16
Rotary Joint
3/4"
OIL
From SunDial MAN
2"
E-04
5"
002-HTF-2"-PN16
1 1/4"
M
2"
F-02
2"
E-03
1/2"
1/2"
SP
Nota 1
PSV
Receiver-2
70 mm
70mm
Nota 2
Vv_M
Receiver-1
70mm
70mm
CATCH POT
FC
04
ON/OFF
M-1
001-HTF-2"-PN16
5"
SunDial-LL
3/4"
Rotary Joint
3/4"
OIL
from BOP
TIT
01
WIT
01
GIT
01
DIT
01
METEOROLOGICAL STATION
NOTE 1: located at the highest point
NOTE 2: vent to safe location
SUNDIAL- LL P&ID

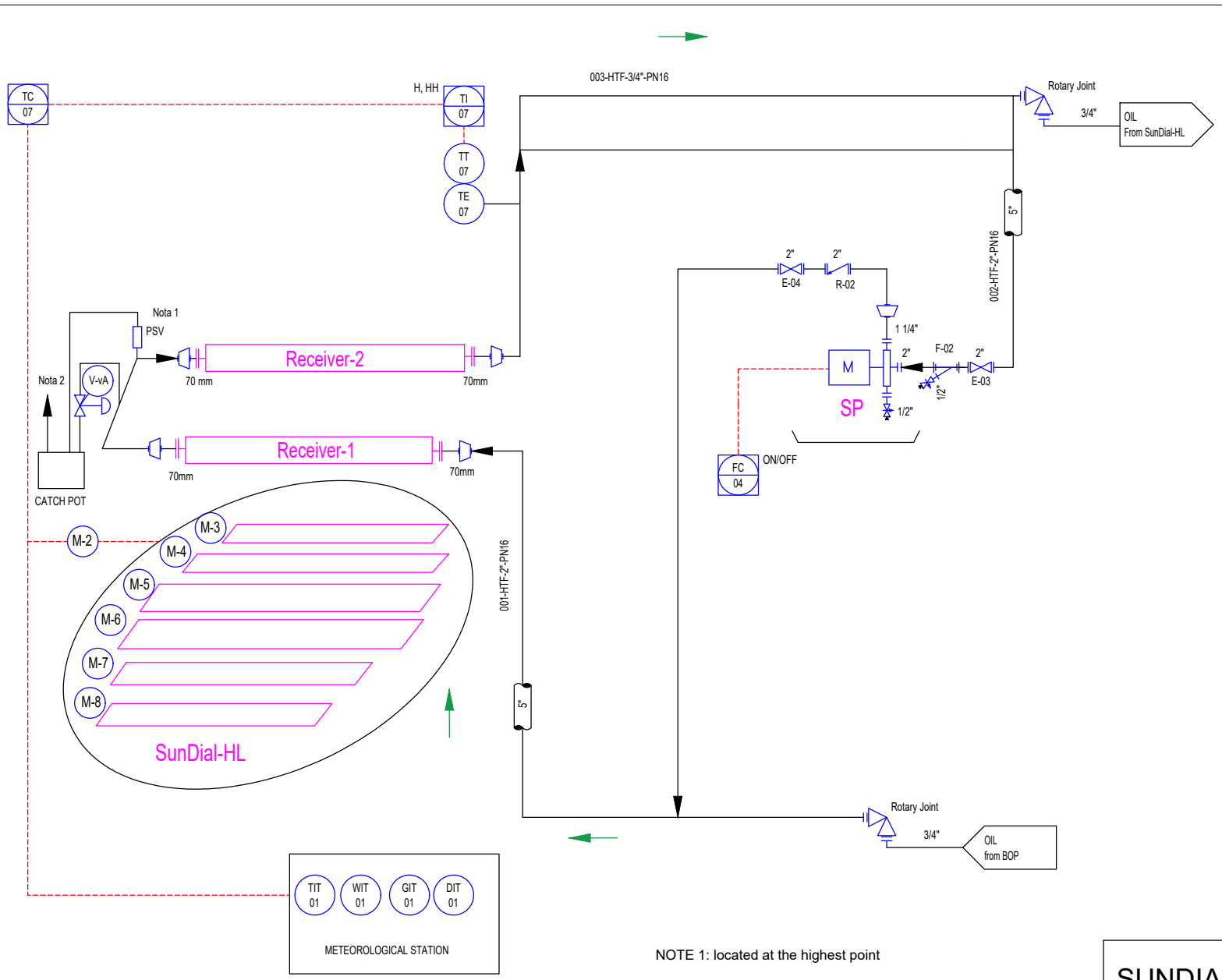

NOTE 1: located at the highest point

NOTE 2: vent to safe location

SUNDIAL- HL P&ID

C - Mechanical design of the installation piping

Piping design conditions

The piping was selected following the European standard DIN or the Spain standard EN 10216-2. The material selected was P265GH, but due to issues in the procurement also P235GH was used. The diameter of the piping was selected by a compromise solution between the pressure drop, which is lower at higher diameters, and the thermal losses, which increase with the diameter. The thermal insulation of 4 inches of thickness was calculated to reduce the thermal losses to the ambient lower than 10% of the power produced by the SunDial. To estimate the heat losses fiberglass with the properties of the commercial rock wool was used. The nominal diameters (ND) selected were 50 for the SunDial recirculation and 20 for the rest of the SunDial piping and the BOP.

The piping thickness (t) selected was standard DIN 2440 and 2448, which are shown in Table C.1. The critical pressure (p_{critical}) was calculated with Eq. C.1 from standard UNE-EN 13480-3. Where f is the material stress at 250 °C, 10 degrees over the maximum operative condition. A forming tolerance of 0.5 mm and DIN 2448 thickness were considered for the calculations. No corrosion thickness was considered because the installation will be used only for the test campaign (two months). Table C.2 illustrates the results where the limit is defined by the lower value of the maximum pressure admitted, which is 8.29 bar.

Table C.1: DIN standard thickness for different nominal diameters

ND	D_o	DIN 2448	DIN 2440
20	26.9	2.3	2.65
25	33.7	2.6	3.25
50	60.3	2.9	3.65

$$p_{\text{critical}} = \frac{2.t.f}{D_0 - t} \tag{C.1}$$

Table C.2: Critical pressure for the piping

Material	f	ND50	ND20
P265GH	114	9.45	16.35
P235GH	100	8.29	14.34

Piping and equipment connections

The system connections were prioritized in the following order, from most preferable to least: welding, flanging, and threading, due to the flammable condition of the thermal oil to avoid leaks. Flanges were used at disconnection points to facilitate maintenance or inspection. The weld connections in small diameters (ND20) are preferred socket welded because is easy to perform the welding, for the larger diameters (ND50) the butt weld is preferred. The threaded

connections, on the other hand, were typically employed at locations with low-pressure and low-temperature requirements. Nevertheless, in some instances, threaded connections were utilized in high-temperature areas due to challenges in procuring specific equipment like pumps, rotary joints, and pressure relief valves. To ensure the integrity of the threaded connections, teflon tape resistant to the design temperature was applied for sealing.

The thermal oil provider recommended the use of a weld neck and raised face flange in combination with a spiral-wound gasket. Consequently, the EN-1092-1 Type 11 PN10-40 standard was applied to the flanges, along with TGS outer rings made of 361L steel and flexible graphite gaskets conforming to EN1514-2 PN10-40 specifications. The bolt loading for gasket compressibility was determined using Equation C.2, which involves multiplying the assembly stress by the gasket service area and then dividing by the number of bolts, in this case, four. The area is defined as the space within the graphite ring and is calculated using Equation C.3, where d_3 represents the exterior diameter and d_2 denotes the interior diameter. The recommended load values are detailed in Table C.3, with the minimum load corresponding to the initiation of gasket sealing and the maximum load indicating potential gasket damage. Lastly, bolts with a property class of 6.8 were chosen to achieve the recommended load, as demonstrated in Table C.4.

$$F_{bolt} = A_{gasket}.S/n_{bolt} \tag{C.2}$$

$$A_{gasket} = \frac{\pi}{4}.({d_3}^2 - {d_2}^2) \tag{C.3}$$

Table C.3: Bolts loading for the graphite gasket compressibility

ND	Graphite gasket Stress [N/mm^2]	Bolts loading [N] 20	50
Minimun	50	9,424.78	24,504.42
Recommend	95	17,907.08	46,558.40
Maximum	180	33,929.20	88,215.92

Table C.4: Bolts maximum loading and torque for different metrics

Property class 6.8	M-12	M-16
Bolt max. Load [N]	26,550.00	50,216.00
Bolt max torque [N.m]	63	156
Bolt applied torque [N.m]	50	150

D - Cost calculation for the different SunDial sizes

This section explains the cost estimation for the larger versions of the SunDial. As the SunDial platform is increased more rail circumference and wheels are required. The circumference and the wheels are added to respect the same distance between wheels in the original SunDial. Also, the inclination of the mirrors and the receiver is maintained. Therefore the highest point of the SunDial is increased. The area of mirrors and the total occupied by the platform is proportionally increased.

The cost for the extended versions was calculated based on the original cost of SunDial 8x8 affected by different factors depending the category with the next Equations:

$$c_{ext,rec} = \frac{L_{ext,rec} \cdot c_{rec}}{A_{ext,ref}} \tag{D.1}$$

$$c_{extLL,trac} = \frac{c_{8mplt}}{A_{extLL,ref}} \tag{D.2}$$

$$c_{extHL,trac} = \frac{c_{8mplt} + c_{8mmir} \cdot \frac{n_{ext,mir}}{n_{8,mir}}}{A_{extHL,ref}} \tag{D.3}$$

$$c_{ext,mir} = \frac{c_{8mir} \cdot \frac{A_{ext,ref}}{A_{8,ref}} \cdot \frac{H_{ext}}{H_8}}{A_{ext,ref}} \tag{D.4}$$

$$c_{ext,htf} = \frac{c_{8rj} + c_{8pip} \cdot \frac{L_{ext,pip}}{L_{8,pip}}}{A_{extHL,ref}} \tag{D.5}$$

$$c_{ext,rails} = \frac{c_{8rails} \cdot \frac{P_{ext,rails}}{P_{8,rails}}}{A_{ext,ref}} \tag{D.6}$$

$$c_{ext,str} = \frac{c_{8w} \cdot \frac{n_{ext,w}}{n_{8,w}} + c_{8str} \cdot \frac{A_{ext,plt}}{A_{8,plt}} \cdot \frac{H_{ext}}{H_8}}{A_{ext,ref}} \tag{D.7}$$

Here c is the cost per reflective area of the extended versions (12x12, 16x16, or 20x20). For all the categories the equations are the same for both SunDials except for the tracking, which is different depending on the SunDial-LL or SunDial-HL. The cost per reflective area of the receiver ($c_{\text{ext,rec}}$), considers the total length of the receiver ($L_{\text{ext,rec}}$) and the cost of the standard evacuated per meter (c_{rec}). The cost per reflective area of the tracking for the SunDial-LL ($c_{\text{extLL,trac}}$) considers the total cost for the tracking in the SunDial 8x8 (c_{8mplt}) divided by the new reflective area because the motors are the same independent of the size of the platform. In the SunDial-HL the tracking cost ($c_{\text{extHL,trac}}$) is split between the cost of the motors required for the platform (c_{8mplt})and the required for the mirrors (c_{8mmir}), the last is affected by the ratio of the number of mirror lines in the extended SunDial-HL versus the SunDial 8. The cost per reflective area of the mirrors ($c_{\text{ext,mirr}}$) considers the ratio of the reflective areas and the height of the collectors. In the HTF category (c_{htf}), the cost of the rotating joints ($c_{\text{8,rj}}$), which are the same number in all the collector sizes, are considered separately from the total cost of the piping ($c_{\text{8,pip}}$) which is affected by the ration of piping

length in the collector. In the rails category ($c_{\text{ext,rails}}$), the ratio of the sum of the perimeters of the rails is used. In the structure category ($c_{\text{ext,str}}$), the cost of the wheels is affected by the ratio of the number of wheels and the rest by the ratio of the total area of the platform and the platform height.

Finally, for the cost of installation 20 % of the extra hours required for the SunDial 12x12, 50 % for the SunDial 16x16, and 75 % for the SunDial 20x20 were considered. In the transport category, the same total cost is considered for the SunDial 12x12, for the SunDial 16x16 the double is considered, and for the SunDial 20x20 four times the cost.

Table D.1: Data for the cost calculation of the different sizes of the SunDial-HL

SunDial- HL	8x8	12x12	16x16	20x20	24x24
Receiver longitude	16	36	64	100	144
Receiver height	2.6	2.9	3.25	3.6	3.95
Piping length	24.0	27.8	37.5	47.2	60.96
Area mirrors	44	99	176	275	396
Mirrors lines	6	9	12	15	18
Area platform	64	144	256	400	576
Number Rails	3	4	6	8	10
Wheels	20	36	84	156	244
Sum radius rails	13.1	22.4	43.3	69.9	102.3
Receiver cost					
Lower	38.9	38.9	38.9	38.9	38.9
Upper	54.5	54.5	54.5	54.5	54.5
Tracking					
Lower	52.9	30.7	21.3	16.2	13.1
Upper	73.4	41.8	28.7	21.7	17.4
Mirrors					
Lower	15.16	17.2	19.3	21.4	23.5
Upper	24.84	28.3	31.7	35.1	38.5
HTF					
Lower	28.3	13.9	9.8	7.5	6.4
Upper	33.5	16.2	11.1	8.3	7.0
Foundation					
Lower	17.1	13.0	14.1	14.6	14.8
Upper	21.5	16.4	17.8	18.4	18.7
Structure					
Lower	39.77	43.70	49.67	55.41	60.73
Upper	58.80	65.33	73.91	82.26	90.20
Installation					
Lower	36.36	19.39	13.64	10.18	8.08
Upper	72.73	38.79	27.27	22.91	18.18
Transport					
Lower	5.68	2.53	2.84	3.64	2.53
Upper	9.20	4.09	4.55	5.82	4.04
Total					
Lower	234.09	179.35	169.59	167.86	168.05
Upper	348.49	265.44	249.54	249.04	248.51

Table D.2: Data for the cost calculation of the different sizes of the SunDial LL

SunDial- LL	8x8	12x12	16x16	20x20
Receiver longitude	16	36	64	100
Receiver height	3.4	4.1	4.8	6.98
Piping	24.0	30.2	40.6	53.96
Area mirrors	47.5	106.9	190	296.9
Mirrors lines	6	9	12	15
Area platform	68.89	155	275.6	430.505
Number Rails	3	4	6	8
Wheels	20	36	84	156
Sum radius rails	13.1	22.4	43.3	69.9
Receiver cost				
Lower	36.0	36.0	36.0	36.0
Upper	50.5	50.5	50.5	50.5
Tracking				
Lower	19.2	8.5	4.8	3.1
Upper	29.7	13.2	7.4	4.8
Mirrors				
Lower	36.38	44.0	51.5	74.9
Upper	51.12	61.8	72.4	105.2
HTF				
Lower	26.2	13.7	9.6	7.7
Upper	31.0	15.8	10.8	8.5
Foundation				
Lower	15.8	12.0	13.1	13.5
Upper	20.0	15.1	16.5	17.0
Structure				
Lower	42.72	49.93	58.95	84.52
Upper	62.59	73.96	87.09	125.43
Installation				
Lower	33.68	17.96	12.63	9.43
Upper	67.37	35.92	25.26	21.22
Transport				
Lower	5.26	2.34	2.63	1.68
Upper	8.53	3.79	4.21	2.69
Total				
Lower	215.28	184.47	189.26	230.90
Upper	320.82	270.17	274.21	335.41

E - Model for the parabolic trough collector

The inclusion of the SolAbs model to the ASTEP system was conducted by connecting the thermal port of the SolAbs to a Modelica Dynamic Pipe, as is described in Figure E.1. The input variables to the SolAbs model are the ambient temperature, the wind velocity, the DNI, and the incident angle. This variable will be introduced to the simulation by a weather table, as in the SunDial model. Furthermore, the defocus controller implemented for the SunDial in Section 3.1.2 was adapted to be applied in the PTC model. In the PTC model, the DNI will be multiplied by the focus variable, calculated by the PI controller.

The incident angle of a PTC collector depends on the orientation of the central axis and can be calculated by Equation E.1 for the East-West orientation and Equation E.2 for the North-South orientation.

$$\theta = arccos\left(\sqrt{1 + cos(\delta)^2 \cdot (cos(\omega)^2 - 1)}\right) \tag{E.1}$$

$$\theta = arccos\left(cos(\delta) \cdot \sqrt{(cos(\phi) \cdot cos(\omega) + tan(\delta) \cdot sen(\phi))^2 + sen(\omega)^2}\right) \tag{E.2}$$

The IAM is estimated by the Equation E.3 with the experimental data provided by Riffelmann [66]. Finally, the parameters introduced in the model are illustrated in Table E.1. The data for the optical properties for the PTC were taken from the experimental studies carried out in the validation of the model in PSA [26].

$$IAM = cos(\theta) \cdot \left(1 - \frac{2 \cdot 10^{-5} \cdot \theta + 3 \cdot 10^{-5} \cdot \theta^2}{cos(\theta)}\right) \tag{E.3}$$

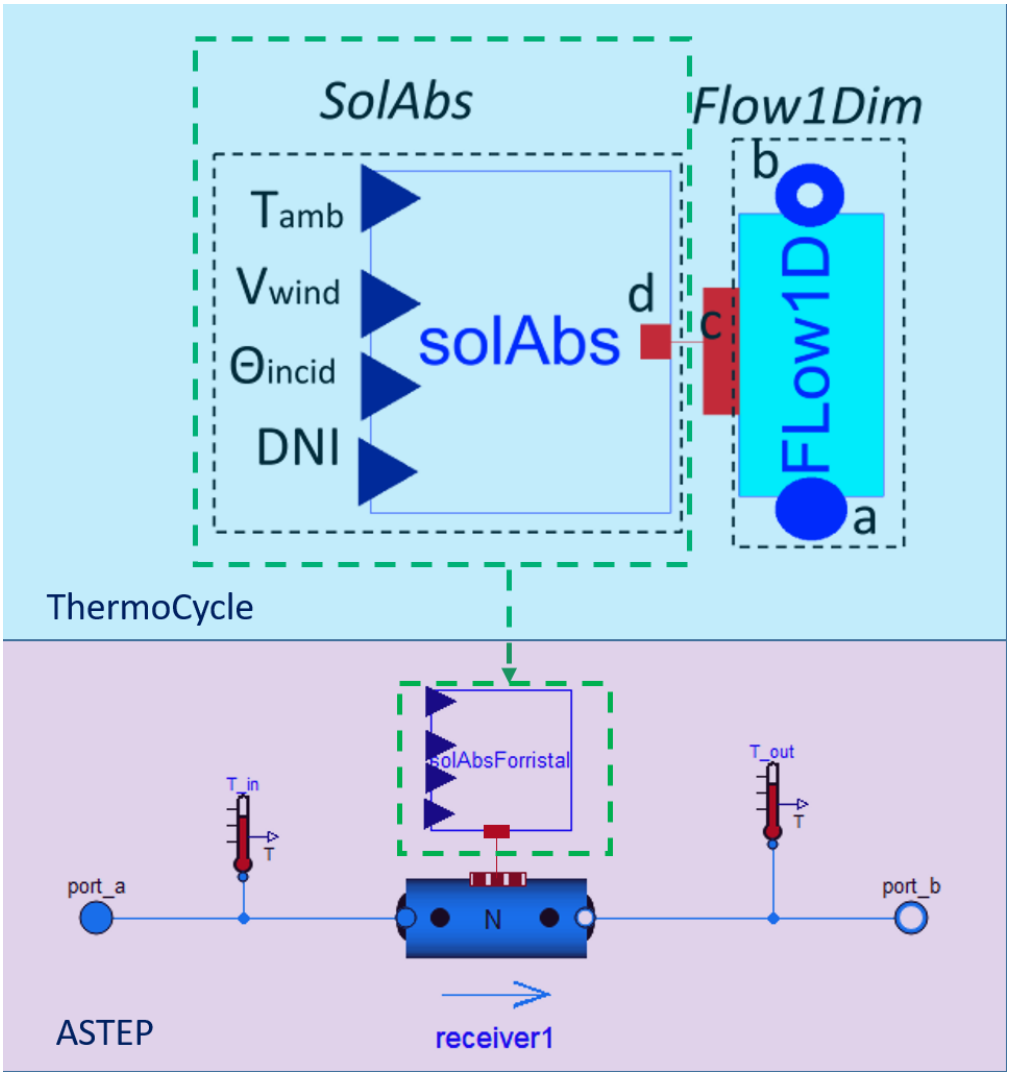

Figure E.1: Insertion of the ThermoCycle Model in ASTEP model.

Table E.1: Parameter for the PTC Dymola model.

Parameter	Value	Unit
L_{rec}	24.5	m
Aperture	7.51	m
D_o	0.07	m
D_i	0.066	m
D_g	0.115	m
k_s	45.5	$W/m \cdot K$
C_s	536	$J/kg \cdot K$
ρ_s	7700	kg/m^3
HCE Shadowing	0.974	
Tracking error	0.994	
Geometry error	0.98	
Mirror reflectivity	0.9388	
Dirt on Mirrors	1	
Dirt on HCE	1	
Unaccounted	0.94	
Glass Transmissivity	0.92	
Glass Absorptivity	0.02	
Glass Emissivity	0.86	
Tube Absorptivity	0.79	